This article has been accepted for publication in a future issue of this journal, but has not been fully edited. Content may change prior to final publication. Citation information: DOI 10.1109/TPEL.2014.2345696, IEEE Transactions on Power Electronics





# An Estimator-Based Distributed Voltage Predictive Control Strategy for AC Islanded Microgrids

Yanbo Wang, Zhe Chen, *Senior Member, IEEE,* Xiongfei Wang, *Member, IEEE,* Yanjun Tian, Yongdong Tan, and Chao Yang

***Abstract*—This paper presents an estimator-based voltage predictive control strategy for AC islanded microgrids, which is able to perform voltage control without any communication facilities. The proposed control strategy is composed of a network voltage estimator and a voltage predictive controller for each distributed generator, where the voltage estimator serves as an essential tool to obtain network voltages response without using communication links, while the voltage predictive controller is able to implement offset-free voltage control for a specified bus. The dynamic performance of the proposed voltage control strategy is analyzed through small signal analysis method, from which the design guideline for the controller parameters is formulated. Furthermore, the robustness of the proposed voltage control strategy is investigated under a series of parameters uncertainties, including the line parameters perturbation, load parameters variation, different disturbance locations, LC filters perturbation, output impedances perturbation and DG unit fault. The simulation and experimental results show that the proposed control approach is able to perform offset-free voltage control without any communication links and has a good capability to reject uncertain perturbations of islanded microgrids.**

***Index Terms*—Distributed voltage predictive control, voltage estimator, dynamic performance, robustness, islanded microgrid.**

## I. Introduction

As the expansion of renewable energy utilization, the small-scale distributed power generation systems such as microgrid [1-2] and virtual power plants [3] have become attractive architectures for future active distribution networks. These small autonomous power systems integrating various forms of Distributed Generation (DG) units and local loads improve the reliability and efficiency of electricity services [4]. A microgrid can be operated flexibly either in a grid-connection mode or in an islanded mode according to the power system conditions [5-6]. During the islanded operation, droop control methods [7-13] are generally employed to automatically assign the active and reactive power among DG units without using communication links. Although the droop control provides the flexibility and reliability for power sharing, it also results in further drawback. The network voltages tend to drop as the droop controllers decrease the terminal voltage of DG units to track the increased reactive power in the presence of load disturbances [14]. These steady-state voltage offsets consequently degrade the voltage quality, and lead to poor performance in load regulation [15]. Note that an improved droop control method with voltage self-restoration [16] has been presented, where voltage-derivative is adopted to perform output voltage restoration. However, the method has a poor control performance in the presence of local disturbances [7] and fails to perform voltage control for different buses in multi-bus islanded microgrids.

To deal with the voltage deviation issue, a number of voltage control methods such as the centralized voltage control in [17] and the decentralized voltage control [18-19] have been developed. The use of several PID control structures for the centralized voltage control in an islanded microgrid are investigated in [20]. A controller design and optimization method using particle swarm optimization algorithms is presented in [14], which are able to coordinate multiple inverter-interfaced DG units against voltage disturbances. A potential function method for centralized secondary voltage control is proposed in [21], where the dynamic voltage set points are commended using communication links within the microgrid. Compared to the centralized control structure, the distributed voltage control methods also earn an increasing concern, which are able to perform voltage regulation locally and quickly so that the whole control system becomes more flexible and reliable. A distributed secondary voltage control strategy based on distributed cooperative control of multi-agent systems is reported in [22], where the one-way communication channels are needed to exchange information among neighboring agents. A distributed control method to regulate output power of multiple photovoltaic generators in a distribution network is addressed in [23]. A second control layer, compensating for voltage deviation caused by the droop control, is proposed in [15]. In [24], an improved droop control method with a capacity of controlling bus voltage is developed for a DC

This work is supported in part by China Scholarship Council and the authors would like to thank the Danish Council for Strategic Research for providing the financial support for the project "Development of a Secure, Economic and Environmentally-friendly Modern Power Systems" (DSF 09-067255). A part of the work has been published on International Power Electronics Conference-ECCE Asia-, Japan, 18-21, May, 2014.

Y. Wang, and Y. Tan are with the Electrical Engineering School, Southwest Jiaotong University, Chengdu 610031, China. (ywa@et.aau.dk; ydtan@swjtu.edu.cn).

Z. Chen, X. Wang, and Y. Tian are with the Department of Energy Technology, Aalborg University, Aalborg 9220, Denmark. (zch@et.aau.dk; xwa@ et.aau.dk; yti@et.aau.dk)

C. Yang is with the college of Electrical Engineering, Chongqing University, Chongqing, 400044, China. (esyangchao@163.com)

microgrid, which uses local controllers and the low bandwidth communication link to exchange information between inverter units. A distributed secondary control approach implementing voltage control and reactive power sharing is proposed in [25]. However, for these voltage control approaches aforementioned, the critical communication links are necessary to acquire voltage responses and send control commands, which undoubtedly bring network-induced side effects such as data drop-out and time delay [25]-[26]. In a multi-bus AC islanded microgrid, when various DG units and loads may be located far away from each other, the complicated communication links make such voltage control schemes much less reliable and flexible. Hence, it would be desirable to avoid using the critical communication channels to improve the voltage control system performance.

State estimation methods [27-30] have been presented as an important approach to extract system dynamics and to reduce communication system burdens. A linear state estimation formulation is addressed in [27], which serves as an effective tool to aid system monitoring, automation and control efforts in smart distribution systems. A survey on state estimation in electric power grids [28] is provided and the impact on state estimation of the technological changes is examined. A Belief Propagation-based distribution system state estimator is presented to alleviate data communication burden in [29], but data acquisition systems require communication links to accomplish the state estimation process. In [30], a linear model-based Kalman state estimation approach is proposed, which operates by using local models of power network associated with a virtual disturbance model. However, it is difficult to estimate network voltages and states of DG units due to the simplified virtual model.

To address these problems aforementioned, a Kalman Filter-Based state estimation method without communication links is proposed to accomplish state estimation in our previous work [31], where the local estimator can dynamically obtain network status. Furthermore, a communication-less distributed voltage control strategy for a multi-bus islanded AC microgrid is proposed in [32], which can implement not only accurate voltage control for a single-bus, but also optimal control for multi-bus. However, whether these model-based state estimation and control methods can work efficiently under model mismatch is not studied yet.

As a matter of fact, for a multi-bus AC islanded microgrid, there exists indeed an inherent modeling error for the microgrid model in comparison to the true microgrid plant. Modeling mismatch resulting from system parameters perturbation has a negative influence on the closed-loop performance [33]-[34]. Therefore, dynamic performance and robustness for the estimator-based voltage control scheme under model mismatch should be further analyzed and investigated.

In the paper, as an extension of the previous work [32], an estimator-based voltage predictive control scheme with rejection capability to parameters perturbation is proposed, and the impact of system uncertainties on the proposed voltage control strategy is discussed in details. The main contributions of this paper are: (1) The critical issues in implementing the communication-less network voltage control are pointed out; (2) The dynamic performance of the proposed voltage controller is analyzed; (3) The robustness of the proposed voltage controller against parameters perturbations is investigated in details.

The rest of paper is organized as follows. In Section Ⅱ, the conventional voltage control approaches are reviewed. In Section Ⅲ, the estimator-based voltage predictive control strategy is proposed, and the concept and principle of the control strategy is given. In Section Ⅳ, the simulations and experiments are presented to validate the proposed control strategy. The conclusions are drawn in Section Ⅴ.

## II. INHERENT DRAWBACKS OF THE CONVENTIONAL VOLTAGE CONTROL APPROACHES

During the islanded operations, network voltages will drop since droop controller decreases voltage to track the increased reactive power in the presence of load disturbances. To compensate for steady-state voltage deviations caused by droop controllers, secondary voltage control [20-22], [25], [35] is adopted to implement voltage restoration. In this section, the conventional voltage control approaches for an AC islanded microgrid are reviewed, including the centralized voltage control [17, 20-21] and the distributed voltage control [22-25], respectively.

### A. *The Centralized Voltage Control Approach*

Fig. 1 illustrates a centralized control-based islanded microgrid configuration, which is composed of multiple DG units and loads. Each DG unit is interfaced to the microgrid by an inverter and controlled by a local power controller. When network voltages drop, the centralized voltage controller [17,20-21] will compensate for the voltage deviation. As shown in Fig. 1, communication links are adopted to obtain voltage responses at different buses. Also, voltage control commands from centralized controller are sent to power controllers by the communication links.

### B. *The Distributed Voltage Control Approach*

Fig. 2 depicts the distributed voltage control approaches [18-19, 22-25]. Compared with centralized voltage controller, the distributed voltage controller carries out control commands locally and quickly. The fault of single distributed voltage controller will not produce a critical influence on the whole system, which thus makes the islanded microgrid more flexible and reliable.

It can be observed that the communication links (even if low bandwidth) are indispensable to support system operation for either the centralized voltage controls or the distributed voltage control. Once communication system fault or data drop-out happens, these control approaches fail to perform voltage regulation. In particular, when various DG units and loads are located far away from each other, the fixed control structures will make islanded microgrids less flexible and reliable [2].

Hence, the paper presents an estimator-based voltage

This article has been accepted for publication in a future issue of this journal, but has not been fully edited. Content may change prior to final publication. Citation information: DOI 10.1109/TPEL.2014.2345696, IEEE Transactions on Power Electronics





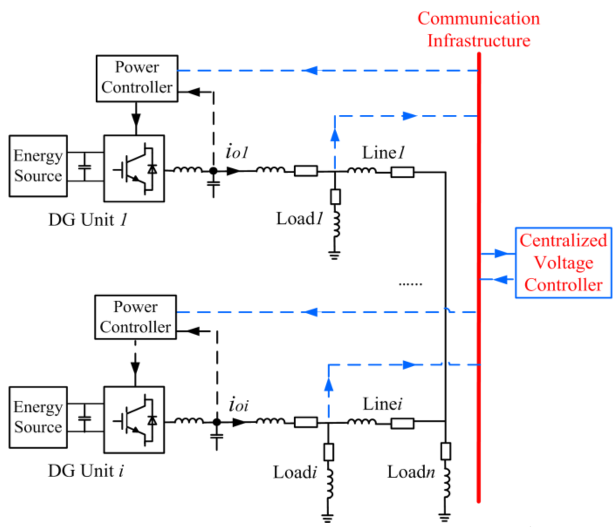


Fig. 1. The centralized control-based islanded microgrid configuration.

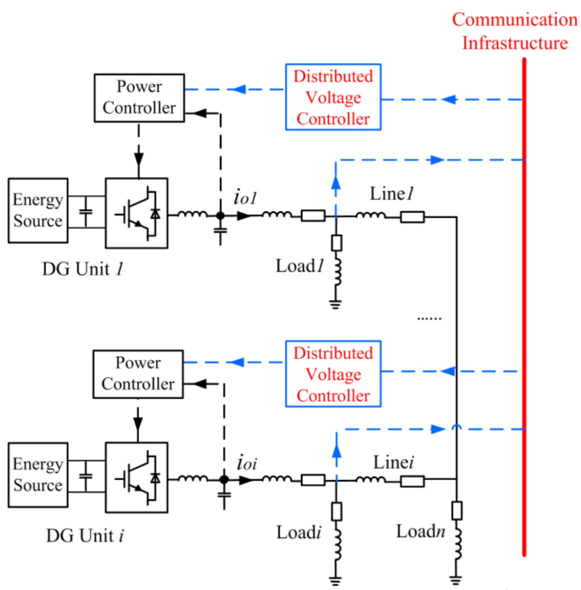


Fig. 2. The distributed control-based islanded microgrid configuration.

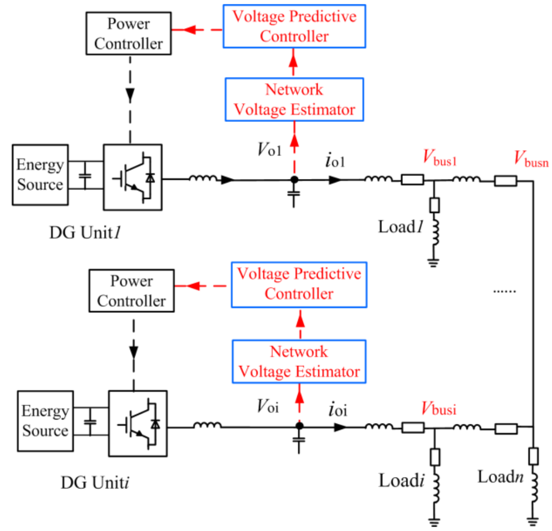


Fig. 3. The proposed estimator control-based voltage control strategy.

control approach more flexible and reliable; (3) The proposed voltage control strategy has a good ability to reject parameters perturbations; (4) The voltage control strategy can be implemented easily due to communication-less operation.

Fig. 4 shows general design flow of the proposed voltage control strategy. To support voltage estimation, the discrete small signal model is first developed to produce voltages response in the presence of load disturbances. Second, with consideration of influences from model mismatch and measurement noises, the disturbance models and noise models are augmented to system model respectively. Then, the network voltage estimator and voltage predictive controller based on the augmented model are presented to generate control commands. Finally, the generated control commands are given to original power controller.

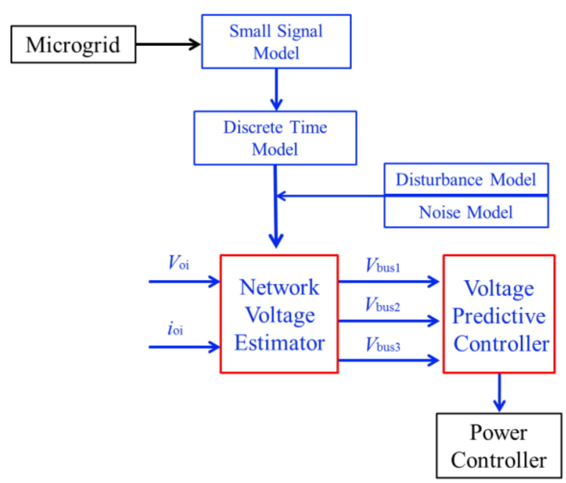


Fig. 4. The design procedures of the proposed control strategy.

control strategy, which is able to perform offset-free voltage control without any communication facilities.

## III. THE PROPOSED ESTIMATOR-BASED VOLTAGE PREDICTIVE CONTROL STRATEGY

Fig. 3 illustrates the block diagram of the proposed estimator-based voltage control strategy, which is composed of the local voltage estimator and the voltage predictive controller respectively. The proposed voltage estimator can obtain dynamically network voltages response based on local voltage and current of each DG unit. And the voltage predictive controller is able to perform offset-free voltage control for a specified bus, even if parameters perturbations happen. Compared with the conventional voltage control approaches, the main benefit of the proposed method is that (1) Each DG unit estimates network voltages response just by local voltage and current itself rather than using communication links; (2) Each voltage predictive controller carries out control commands locally so that the voltage

### *A. The Small Signal Model of an AC Islanded Microgrid.*

To exemplify the proposed estimator-based voltage control strategy, the small signal model of a multi-bus islanded AC microgrid is developed. Some previous small signal models, including power controller, voltage controller, current controller, network as well as loads, have been presented in

This article has been accepted for publication in a future issue of this journal, but has not been fully edited. Content may change prior to final publication. Citation information: DOI 10.1109/TPEL.2014.2345696, IEEE Transactions on Power Electronics





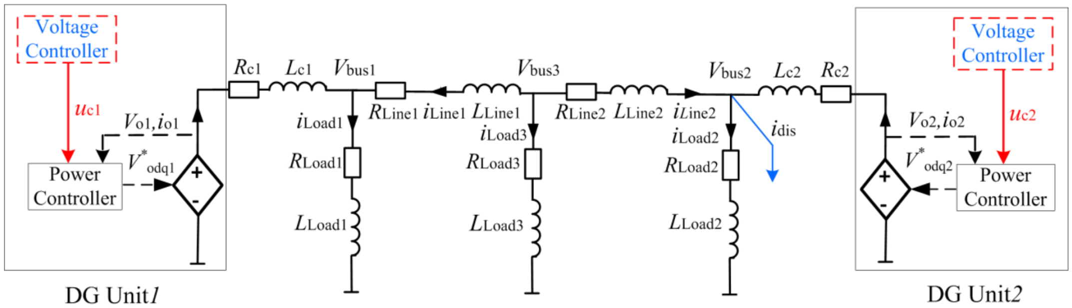


Fig. 5. The small signal model of an AC microgrid.

[2],[36]-[37]. However, the virtual resistors [2],[16] defining network voltages between nodes and ground lead to inaccurate voltage responses and have a negative influence on dynamic stability of whole system [2]. To avoid adverse influences of the virtual resistors, network performances are modeled by linear combination of system states.

In the small signal model to be founded, DG unit can be represented by a controllable voltage source [16] with the assumption that current loop and voltage loop have much faster dynamics than power controller. And the small signal dynamics of each DG unit are formulated in individual frame itself (d-q). All the DG units, network dynamic and loads dynamic are represented on the common reference frame (D-Q). To found overall model on the common reference frame, the reference frame of one DG unit is considered as common reference frame (D-Q) with the rotating frequency of $\omega_{com}$, and all the other inverters are transferred to the common frame by using transformation equation [2] as (1).

$$\begin{bmatrix} f_D \\ f_Q \end{bmatrix} = \begin{bmatrix} \cos(\delta_i) & -\sin(\delta_i) \\ \sin(\delta_i) & \cos(\delta_i) \end{bmatrix} \begin{bmatrix} f_d \\ f_q \end{bmatrix} \tag{1}$$

The angle of the *i*th DG reference frame with respect to the common reference frame, is given in (2), thus $\delta_i$ and $\delta_0$ expresses angle and initial angle between reference frame of each inverter itself and common frame respectively,

$$\delta_i = \int (\omega_i - \omega_{com})dt + \delta_0 \tag{2}$$

The power controller, shown in Fig. 6, adopts droop control

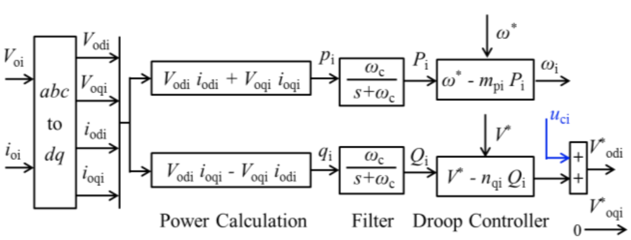


Fig. 6. The power controller of DG unit.

method and provides the voltage references $V^*_{odqi}$ to controllable voltage source, along with output angle frequency $\omega_i$ of inverter. The average active power $P_i$ and reactive power $Q_i$ are obtained respectively from instantaneous power passing low-pass filters as (3) and (4). $\omega_c$ is cut-off frequency of low-pass filter.

$$P_i = \frac{\omega_c}{s+\omega_c} p_i \tag{3}$$

$$Q_i = \frac{\omega_c}{s+\omega_c} q_i \tag{4}$$

And instantaneous active $p_i$ and reactive power $q_i$ can be represented in d-q rotating frame as (5) and (6):

$$p_i = V_{odi} i_{odi} + V_{oqi} i_{oqi} \tag{5}$$

$$q_i = V_{odi} i_{oqi} - V_{oqi} i_{odi} \tag{6}$$

$V_{odqi}$ and $i_{odqi}$ are output voltage and current of *i*th DG unit on individual frame (d-q). The conventional active power-frequency (*P*-*f*) and reactive power-voltage (*Q*-*V*) droop control method [2] for paralleled inverters operation can be represented as (7) and (8), respectively.

$$\omega_i = \omega^* - m_{pi} P_i \tag{7}$$

$$V^*_{odi} = V^* - n_{qi} Q_i \tag{8}$$

,where $m_{pi}$, $n_{qi}$ are droop coefficients of *i*th DG unit. Generally, secondary voltage control input can be embedded into droop controller [7] to perform voltages restoration so that voltage control can be achieved locally and quickly. To analyze influence of the proposed voltage controller on system dynamic, the voltage control input is embedded and integrated to the small signal model as Fig. 5.

Further, the reactive power-voltage (*Q*-*V*) droop control method with consideration of voltage control can be rewritten as (9) by (8), shown in Fig. 6.

$$V^*_{odi} - u_{ci} = V^* - n_{qi} Q_i \tag{9}$$

Then, the voltage small signal dynamic is represented as (10) by combing and linearizing (4) and (9)

$$\Delta \dot{V}^*_{odi} = -n_{qi}\omega_c \Delta q_i - \omega_c V^*_{odi} + \omega_c \Delta u_{ci} \tag{10}$$

Notice that $u_{ci}$ is responsible for regulate terminal voltage of DG unit, which is introduced to compensate voltage deviation caused by droop controller [7, 15, 25].

The current dynamics of individual inverter in d-q frame can be formulated as (11) and (12) according to KCL in Fig. 5:

$$\dot{i}_{odi} = -\frac{R_{ci}}{L_{ci}} i_{odi} - \omega_i i_{oqi} + \frac{1}{L_{ci}} V_{odi} - \frac{1}{L_{ci}} V_{busDi} \tag{11}$$

$$\dot{i}_{oqi} = -\frac{R_{ci}}{L_{ci}} i_{oqi} - \omega_i i_{odi} + \frac{1}{L_{ci}} V_{oqi} - \frac{1}{L_{ci}} V_{busQi} \tag{12}$$

Sequentially, the small signal current dynamic is given by

This article has been accepted for publication in a future issue of this journal, but has not been fully edited. Content may change prior to final publication. Citation information: DOI 10.1109/TPEL.2014.2345696, IEEE Transactions on Power Electronics





$$\Delta \dot{i}_{odqi} = A_{curi1}\Delta\omega_i + A_{curi2}\Delta V_{odqi} + A_{curi3}\Delta i_{odqi} + B_{curi}\Delta V_{busi} \quad (13)$$

where $A_{curi1}, A_{curi2}, A_{curi3}, B_{curi}$ are current parameters matrixes, given in appendix.

Now, overall small signal dynamics of each DG unit can be obtained by combing (2)-(13):

$$\Delta \dot{x}_{invi} = A_{invi}\Delta x_{invi} + B_{invi}\Delta V_{busi} + B_{ci}\Delta u_{ic} \quad (14)$$

Further, the combined small signal model of all the inverter is shown as (15):

$$\Delta \dot{x}_{inv} = A_{inv}\Delta x_{inv} + B_{inv}\Delta V_{bus} + B_c\Delta u_c \quad (15)$$

where $\Delta x_{invi} = [\Delta\delta_i, \Delta P_i, \Delta Q_i, \Delta V^*_{odi}, \Delta i_{odi,} \Delta i_{oqi}]^T$, $\Delta V_{busi} = [\Delta V_{busDi} \quad \Delta V_{busQi}]^T$, $\Delta V_{bus} = [\Delta V_{bus1} \cdots \quad \Delta V_{busi}]^T$, $\Delta V_{bus}$ is bus voltage vector. The parameters matrixes $A_{invi}, B_{invi}, B_{ci}$ are given in details in appendix. The modelling procedure of DG unit also can be referred in [2].

Similarly, the small signal model of lines currents can be formulated as on a common reference frame (D-Q):

$$\Delta \dot{i}_{LineDQ} = A_{Line}\Delta i_{LineDQ} + B_{Line1}\Delta i_{oDQ} + B_{Line2}\Delta \dot{i}_{oDQ} + B_{Line3}\Delta\omega_1 + B_{dis}\Delta i_{disDQ} \quad (16)$$

And the small signal model of loads currents on the common frame can be represented and linearized according to KCL in Fig. 5 as

$$\Delta \dot{i}_{LoadDQ} = A_{Load}\Delta i_{LoadDQ} + B_{Load1}\Delta i_{LineDQ} + B_{Load2}\Delta i_{oDQ} + B_{Load3}\Delta \dot{i}_{oDQ} + B_{Load4}\Delta\omega_1 + B_{dis2}\Delta i_{disDQ} \quad (17)$$

As shown in Fig. 5, bus voltages can be represented according to KCL as (18):

$$\begin{aligned} V_{bus1} &= R_{Load1}(i_{o1} + i_{Line1}) + L_{Load1}\frac{d(i_{o1} + i_{Line1})}{dt} \\ V_{bus2} &= R_{Load2}(i_{o2} + i_{Line2} - i_{dis}) + L_{Load2}\frac{d(i_{o2} + i_{Line2} - i_{dis})}{dt} \\ V_{bus3} &= R_{Load3}(-i_{Line1} - i_{Line2}) + L_{Load3}\frac{d(-i_{Line1} - i_{Line2})}{dt} \end{aligned} \quad (18)$$

By transforming (18) onto D-Q common frame and linearizing them, voltages equation considering load disturbances can be obtained as (19)

$$\Delta V_{busDQ} = C_{vol}[\Delta x_{inv}] + C_{vol2}\begin{bmatrix}\Delta i_{LineDQ} \\ \Delta i_{LoadDQ}\end{bmatrix} + D[i_{disDQ}] \quad (19)$$

Note that network voltages, in practice, can be represented as linear combination of certain states.

$L_{loadi}$ and $R_{loadi}$ are inductance and resistance of *i*th load; $i_{LineDQi}$ and $i_{LoadDQi}$ are current of *i*th line and *i*th load on common frame (D-Q). $C_{vol}$, $C_{vol2}$, $D$, $A_{Line}$, $B_{Line1}$, $B_{Line2}$, $B_{Line3}$, $B_{dis}$, $A_{Load}$, $B_{Load1}$, $B_{Load2}$, $B_{Load3}$, $B_{Load4}$, $B_{dis2}$ are parameters matrixes regarding bus voltages, lines and loads, shown in Appendix. $i_{disDQ}$ is unknown load disturbance. The influence of disturbance on system dynamic will be further discussed.

Finally, an overall model including inverters, loads, network with consideration of load disturbance and voltage control dynamic in an islanded microgrid by combining (15), (16), (17) and (19) can be rewritten as

$$\begin{aligned} \Delta \dot{x} &= A\Delta x + B\Delta i_{dis} + B_c\Delta u_c \\ \Delta y &= C\Delta x + D\Delta i_{dis} \end{aligned} \quad (20)$$

$\Delta x$ is overall state vector of whole microgrid, $\Delta x = [\Delta x_{inv1}, \Delta x_{inv2}, \Delta i_{line1}\Delta i_{line2}, \Delta i_{load1}, \Delta i_{load2}, \Delta i_{load3}]$ . The parameters matrixs $A, B, B_c, C, D$ are given in appendix.

### B. *The Discrete Time Model.*

An important step for the proposed voltage predictive control strategy is determining discrete time model, which is developed to support the model predictive control-based control technology [34]. The resulting discrete time model is obtained from small signal model according to (20) as (21):

$$\Delta x(k+1) = A_d\Delta x(k) + B_d\Delta i_{dis}(k) + B_{cd}\Delta u_c(k) \quad (21)$$

$$\Delta y(k) = C_d\Delta x(k) + D_d\Delta i_{dis}(k) \quad (22)$$

The matrixes $A_d, B_d, B_{cd}, C_d, D_d$ are obtained though Euler discretization. (21)-(22) are well-established relationship between internal states $\Delta x(k)$, voltage control inputs $\Delta u_c(k)$, load disturbances $\Delta i_{dis}(k)$ and system output $\Delta y(k)$. Note that output of the system can be divided into measured output and unmeasured output in (22). Load changes are then considered as unknown disturbances. And the details about disturbance modeling and rejection will be discussed later in the paper.

The discrete time model is adopted to generate output responses and support voltage estimation in the presence of load disturbances. To permit a simpler representation, sign' $\Delta$' in increment function is omitted in the following contents.

### C. *The Network Voltage Estimator.*

To lessen communication system burden and improve the reliability and flexibility of voltage control approaches, a network voltage estimator is proposed to obtain voltages response instead of the conventional communication facilities.

(1) Disturbance Model Augmentation

Generally, model mismatch resulting from parameters perturbations is inevitable in real plant. The disturbance model [38]-[40] always can be augmented to original plant model to reject model uncertainties and improve system robustness according to internal model principle [41]. Thus, disturbance model is able to provide primarily a support to perform offset-free control for a specified bus when parameters perturbation happens. In a multi-bus islanded microgrid, the model uncertainties resulting from line parameters perturbation, load parameters perturbation, different disturbance locations, LC filters perturbation, output impedances perturbation and DG unit fault, in fact, lead to voltage control error. To guarantee offset-free voltage control for the specified bus, the discrete time model founded as (21) would be augmented with disturbance models. Load changes are modeled as step-like disturbance sources. In the case analyzed, the disturbance models that includes input and output disturbance are proposed to shape the disturbance

This article has been accepted for publication in a future issue of this journal, but has not been fully edited. Content may change prior to final publication. Citation information: DOI 10.1109/TPEL.2014.2345696, IEEE Transactions on Power Electronics





sources as (23)-(24). And closed-loop performance of the controller is associated with the disturbance model.

$$x_{dis}(k+1) = A_{dis}x_{dis}(k) + B_{dis}w_{dis}(k) \quad (23)$$

$$i_{dis}(k) = C_{dis}x_{dis}(k) + D_{dis}w_{dis}(k) \quad (24)$$

where $A_{dis}, B_{dis}, C_{dis}, D_{dis}$ are parameter matrixes of the disturbance model, given in appendix. Furthermore, system model can be represented by combining (21)-(24):

$$\begin{bmatrix} x(k+1) \\ x_{dis}(k+1) \end{bmatrix} = \begin{bmatrix} A_d & B_dC_{dis} \\ O & A_{dis} \end{bmatrix}\begin{bmatrix} x(k) \\ x_{dis}(k) \end{bmatrix} + \begin{bmatrix} B_dD_{dis} \\ B_{dis} \end{bmatrix} w_{dis}(k) + \begin{bmatrix} B_{cd} \\ O \end{bmatrix} u_c(k) \quad (25)$$

$$y(k) = \begin{bmatrix} C_d & C_{dis}D_d \end{bmatrix}\begin{bmatrix} x(k) \\ x_{dis}(k) \end{bmatrix} + D_dD_{dis}w_{dis}(k) \quad (26)$$

It can be observed that $B_dC_{dis}, C_{dis}D_d$ determines the effect of the disturbance model on system states and output.

(2) Measurement Noise Model Augmentation.

In addition, the measured output is usually corrupted by measurement noises such as sampling errors. To imitate sensors noise, the measurement noise models are also augmented to output channels, which can be represented in a state space model as (27)-(28).

$$x_m(k+1) = A_mx_m(k) + B_mw_m(k) \quad (27)$$

$$m(k) = C_mx_m(k) + D_mw_m(k) \quad (28)$$

$$y_m(k) = C_dx(k) + D_di_{dis}(k) + m(k) \quad (29)$$

Then, noises are added to the measured outputs $y_m$ for imitating measurement environment as (29). $A_m, B_m, C_m, D_m$ are parameters matrixes of the measurement noise model.

Now, an overall model combining full states, disturbances and measurement noise can be represented by combining (25)-(29) as follows:

$$x_T(k+1) = A_ox_T(k) + B_ou_c(k) + W_ow_T(k) \quad (30)$$

$$y_m(k) = C_ox_T(k) + D_ow_T(k) \quad (31)$$

$x_T = \begin{bmatrix} x & x_{dis} & x_m \end{bmatrix}^T$, $A_o = \begin{bmatrix} A_d & B_dC_{dis} & O \\ O & A_{dis} & O \\ O & O & A_m \end{bmatrix}$, $B_o = \begin{bmatrix} B_{cd} \\ O \\ O \end{bmatrix}$, $C_o = \begin{bmatrix} C_d & C_{dis}D_d & C_m \end{bmatrix}$, $D_o = \begin{bmatrix} D_dD_{dis} & D_m \end{bmatrix}$, $W_o = \begin{bmatrix} B_dD_{dis} & O \\ B_{dis} & O \\ O & B_m \end{bmatrix}$, $w_T = \begin{bmatrix} w_{dis}(k) & w_m(k) \end{bmatrix}^T$. The disturbance and noise model are driven by the Gaussian noise $w_{dis}(k)$ and $w_m(k)$. The augmented version of system model will be concerned later.

(3) The Network Voltage Estimator.

Once the aforementioned augmentation model is applicable, the network voltage estimator can be further developed, which implements voltage estimation by Kalman-Filter method. Since unknown disturbances are not directly measurable, the only indication is its effect on the measured output (local voltage and current responses of each DG unit). Also, voltage control input has an influence on system dynamic. Therefore, the inputs of each estimator is local voltage and current as well as its voltage control commands as shown in Fig. 7, where overall states can be updated and revised continuously via these information update. Then, each DG unit can dynamically estimate network voltages of the whole islanded microgrid.

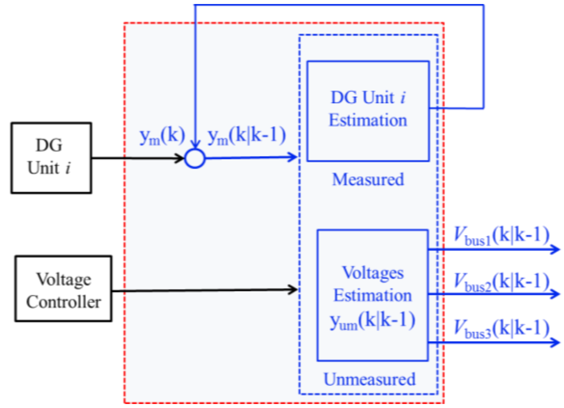


Fig. 7. The operation principle of network voltage estimator.

The principle of voltage estimator is depicted as Fig. 7. Note that the proposed estimator in practice is a steady-state Kalman Filter which estimates plant states and the unknown network voltages by measured information. With assumption that (*Co*, *Ao*) is detectable for augmentation model (30)-(31), the full state estimation equation could be given by

$$\begin{bmatrix} x(k|k) \\ x_{dis}(k|k) \\ x_m(k|k) \end{bmatrix} = \begin{bmatrix} x(k|k-1) \\ x_{dis}(k|k-1) \\ x_m(k|k-1) \end{bmatrix} + \begin{bmatrix} K_1 \\ K_2 \\ K_3 \end{bmatrix}\left(y_m(k) - y_m(k|k-1)\right) \quad (32)$$

$\begin{bmatrix} K_1 & K_2 & K_3 \end{bmatrix}^T$ is the Kalman gain [42], which is the solution of Ricatti matrix equation. Then, the state update equation and estimated output with voltage control action are given respectively as (33) and (34) from (30) and (31)

$$\begin{bmatrix} x(k+1|k) \\ x_{dis}(k+1|k) \\ x_m(k+1|k) \end{bmatrix} = A_o\begin{bmatrix} x(k|k) \\ x_{dis}(k|k) \\ x_m(k|k) \end{bmatrix} + B_ou_c(k) \quad (33)$$

$$y_m(k|k-1) = C_o\begin{bmatrix} x(k|k-1) \\ x_{dis}(k|k-1) \\ x_m(k|k-1) \end{bmatrix} \quad (34)$$

These estimated states are updated and compensated continuously via update of the measured voltage and current of each DG unit as well as the commands from the voltage controller. Then, the state estimation equation can be rewritten by combing (30)-(34) as follows:

$$x_T(k+1|k) = A_Tx_T(k|k-1) + B_Ty_m(k) + B_ou_c(k) \quad (35)$$

where $A_T = A_o - A_o * K_T * C_o$, $B_T = A_o * K_T$, $K_T = \begin{bmatrix} K_1, K_2, K_3 \end{bmatrix}^T$. Meanwhile, the estimated output equation can be divided into two parts as (36) and (37) respectively, including measured output (local voltage and current) and unmeasured output (network voltages).

$$y_m(k|k-1) = C_{om}x(k|k-1) \quad (36)$$

$$y_{um}(k|k-1) = C_{oum}x(k|k-1) \quad (37)$$

As shown in Fig.7, measured states vector $y_m(k) = \left[V_{odi}(k), i_{odi}(k), i_{oqi}(k),\right]$ and voltage control input are seen as estimator inputs, while estimated states vector

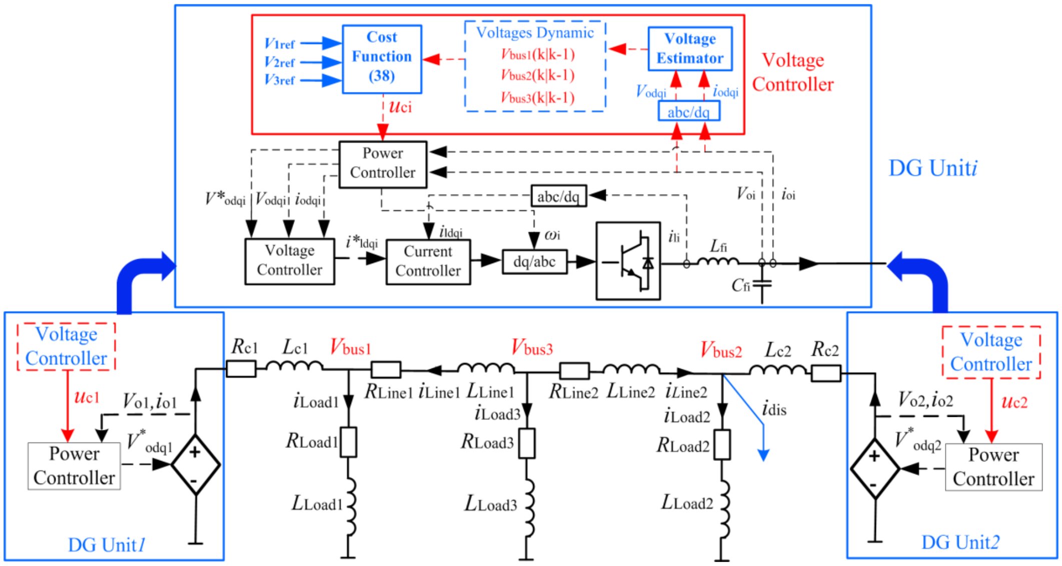


Fig. 8. The block diagram of the proposed voltage predictive controller.

$y_m(k|k-1)=[V_{odi}(k|k-1), i_{odi}(k|k-1), i_{oqi}(k|k-1)]^T$ and estimated voltages vector $y_{um}(k|k-1)=[V_{bus1}(k|k-1)\quad V_{bus2}(k|k-1)\quad V_{bus3}(k|k-1)]^T$ are viewed as estimator outputs.

*D. The Voltage Predictive Controller.*

Once the discrete time model and network voltage estimators are founded, the proposed voltage predictive controller is a following critical step. The desired behavior of proposed voltage controller is formulated as an optimal cost function that minimizes voltage error at specified bus. As it is known, it's impossible to hold all the bus voltages at their set points due to inherent circuit configuration. Therefore, when there are several voltages to be controlled, it should be set priority so that controller can hold the most important voltage at its set point, allowing others varying within an accepted range. In the paper, cost function computing the control commands is defined to hold the bus3 voltage at its set point as shown in Fig. 8. Thus the main quantity to be weighted is voltage error at bus3. Once the voltages estimator will have estimated voltages response, the voltage predictive controller then computes control commands according to these estimated voltage information, where offset-free control for bus3 can be implemented. The control commands are obtained by computing optimization cost function to be minimized, which can be formulated as (38):

$$\min_{\Delta u(k|k),\cdots,\Delta u(m-1+k|k)} J=\left\{\sum_{i=0}^{p-1}\left(\sum_{j=0}^{n_b}(w_{bj}(V_{busj}(k+i+1|k)-V_{jref}))^2+\sum_{j=1}^{n_c}(w_{cj}\Delta u_{cj}(k+i|k))^2\right)\right\} \tag{38}$$

In the cost function, $w_{bj}, w_{cj}$ are weights for network voltages at different buses and control increments, respectively; $p$ is prediction horizon; $n_b=3$ is number of bus; $n_c=2$ is number of voltage control input; $V_{busj}(k+i+1|k)$ denotes the voltages information predicted for time $k+i+1$ based on the measured information available at time $k$. $V_{jref}\ (j=1,2,3)$ are set to 0 (initial equilibrium state defined in origin).

When computing is finished, the each voltage controller sends control commands to its power controller and operates with the control commands until next sampling update. Periodically, the controller obtains new voltages estimation due to measurement feedback and consequently revises its original control plan. Then, the voltage control commands are provided to compensate for the deviation between estimated voltage and reference values. The process repeats independently by voltage controller of each DG unit.

In the voltage controller, an aggressive control increment must be penalized to avoid instant reactive power fluctuation, in which the relationship between the voltage control commands and reactive power dynamic has been established as (9) in SectionIII.A. And it is worth noting that the weight coefficients have a dramatic influence on the closed-loop dynamic performance, which will be analyzed in details later. Besides, another important parameter of the cost function is the length $p$ of the prediction horizon, which is the number of prediction steps. In the implementation of simulations and experiments, it has been chosen that $p=10$. It is the control horizon that is also an essential parameter associated with control commands but not occur in cost function. In the implementation, the control horizon has been chosen that $m=2$ in the paper, which means control inputs are executed during the time span from $k$ to $k$+2 when predicting system dynamics, where $k$ is the sampling instant. In general, the control horizon $m$ should be chosen as small as possible to reduce the computational effort [34], [43]-[44].

The estimator-based voltage control strategy has an attractive advantage that the voltage controller of each DG unit is completely independent without communication links. Thus it provides flexibility and reliability due to communication-less operation.

This article has been accepted for publication in a future issue of this journal, but has not been fully edited. Content may change prior to final publication. Citation information: DOI 10.1109/TPEL.2014.2345696, IEEE Transactions on Power Electronics



### E. The Dynamic Performance Analysis

To investigate the relationship between controller parameters and dynamic performance, the dynamic performance is analyzed in details. In the case analyzed, the dynamic performance of the developed voltage controller is investigated by checking the positions of poles when adjusting weights in the proposed cost function.

As depicted in Fig. 9(a), the closed-loop poles are plotted when modifying bus3 voltage error weight of DG1 controller in cost function. Note that 22 poles can appear in pole map since the whole system has 22 orders, but just a real pole is sensitive highly to the weight variation, where it moves towards origin (improving dynamic response) as bus3 voltage weight increases. Also, dynamic performance for modifying voltage control increment weight of DG1 controller is depicted in Fig. 9(b), where one real pole and one complex conjugate pole pair are sensitive for the weight variation in the case analyzed. With the increase of voltage control increment weight, the real pole and conjugate pole pair are driven to move from origin towards one inside unit cycle, slowing down the speed response for the whole system. Similarly, as shown in Fig. 10(a), dynamic variation of a real pole is illustrated when increasing bus3 voltage error weight of DG2 controller. It can be observed that the real pole moves towards origin, thus system has a much faster dynamic response. Further, a real pole, together with a conjugate pole pair varies from original point towards one inside unit cycle, shown in Fig. 10(b).

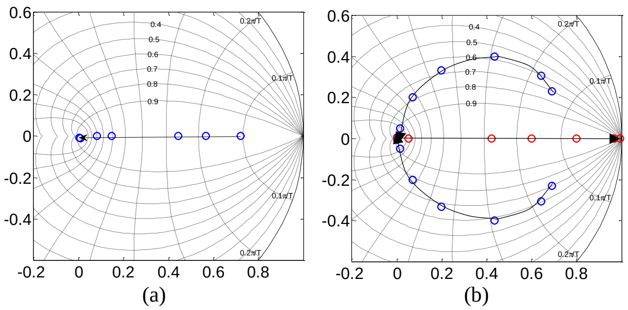

Fig. 9. The poles map for weight variation of DG1 controller. (a) The bus3 voltage weight $w_{b3}$(DG1)= 50, 80, 150, 200, 500, 800, 1000. (b) The control increment weight $w_c$(DG1)= 0.1, 1, 5, 10, 20, 50, 200.

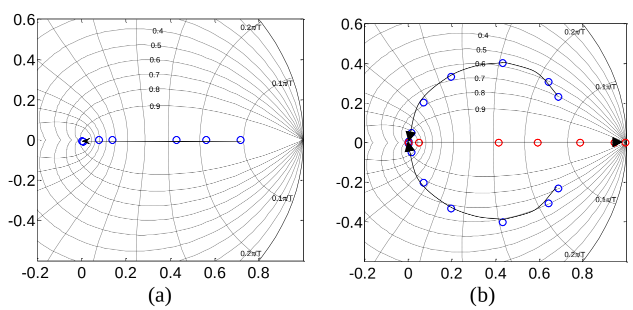

Fig. 10. The poles map for weight variation of DG2 controller. (a) The bus3 voltage weight $w_{b3}$(DG2)= 50, 80, 150, 200, 500, 800, 1000. (b) The control increment weight $w_c$(DG2)= 0.1, 1, 5, 10, 20, 50, 200.

The analysis conclusions are drawn that (1) A real pole is sensitive highly to variation of bus3 voltage weight. With the increase of it, dynamic response can be improved; (2) A real pole, along with a conjugate pole pair, is sensitive to variation of voltage control increment. And the less aggressive voltage control increment, the slower dynamic response.

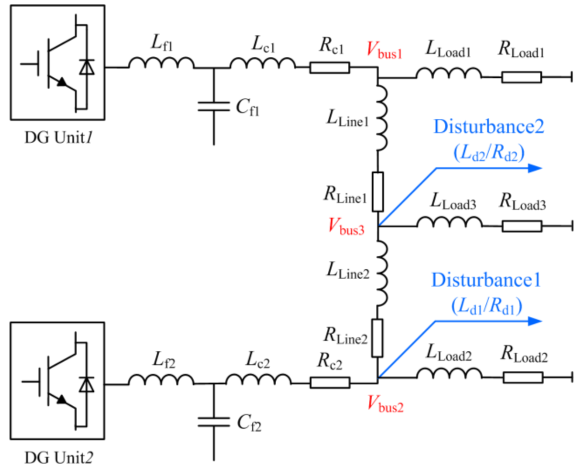


Fig. 11. The hardware photo of the experiment setup.

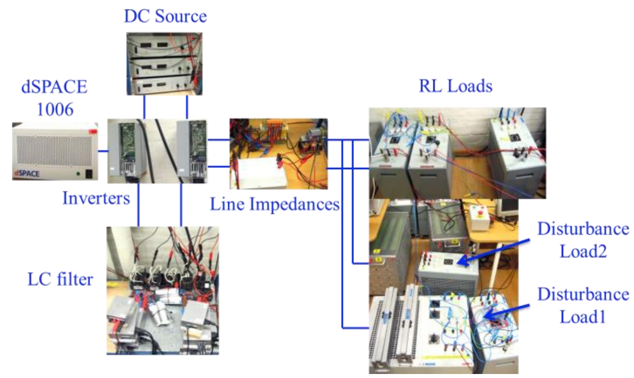


Fig. 12. The hardware photo of the experiment setup.

## IV. SIMULATION AND EXPERIMENTAL VERIFICATION

In order to verify effectiveness of the proposed estimator-based voltage predictive control strategy, the simulations in MATLAB/Simulink and experiments are conducted respectively for a three phase 50 Hz islanded microgrid. As depicted in Fig. 11, the system consists of two inverters in parallel operation and three loads. And the photo of the experiment hardware is shown in Fig. 12. The whole platform of the islanded microgrid is controlled by dSPACE 1006. As mentioned in section I, the robustness of the proposed controller to parameters perturbations is an essential issue. In the paper, to perform offset-free voltage control for bus3 under parameters perturbations, the disturbance models are augmented to the proposed controller.

The simulation and experimental verifications are composed of 7 cases respectively. The case1 is adopted to validate effectiveness of the proposed voltage control strategy. Furthermore, the robustness investigation under parameters perturbations consists of following six cases. The case2 is to study the influence of line parameters perturbations on robustness of controller. The case3 investigates robustness of the controller when load parameters vary. The case4 studies

This article has been accepted for publication in a future issue of this journal, but has not been fully edited. Content may change prior to final publication. Citation information: DOI 10.1109/TPEL.2014.2345696, IEEE Transactions on Power Electronics





TABLE I
PARAMETERS FOR SIMULATION AND EXPERIMENT

| Parameters | Value | Parameters | Value |
|---|---|---|---|
| $L_{f1}/L_{f2}$ | 1.5mH/1.5mH | $L_{Line1}/R_{Line1}$ | 2mH/0.2Ω |
| $C_{f1}/C_{f2}$ | 25μF/25μF | $L_{Line2}/R_{Line2}$ | 2mH/0.2Ω |
| $L_{c1}/L_{c2}$ | 1.8mH/1.8mH | $w_{b3}$(DG1/DG2) | 1000 |
| $m_{p1}/m_{p2}$ | 2.5e-5/1e-4 | $w_{c2}$(DG1/DG2) | 0.1 |
| $n_{q1}/n_{q2}$ | 1e-3/1e-3 | (Simulation) $L_{d1}/R_{d1}$ | 50mH/10Ω |
| Inverter Rate | 10kW | | |
| Switch Frequency | 10k | (Experiment) $L_{d1}/R_{d1}$ | 70mH/10Ω |

TABLE II
PARAMETERS FOR ROBUSTNESS INVESTIGATION

| Case | Parameters | Original Model | Perturbation Plant |
|---|---|---|---|
| 2 | $L_{Line1}/R_{Line1}$ | 2mH/0.2Ω | 3.6mH/0.2Ω |
| | $L_{Line2}/R_{Line2}$ | 2mH/0.2Ω | 3.6mH/0.2Ω |
| 3 | $L_{Load1}/R_{Load1}$ | 155mH/64.5Ω | 145mH/64.5Ω |
| | $L_{Load2}/R_{Load2}$ | 156mH/64Ω | 146mH/64Ω |
| | $L_{Load3}/R_{Load3}$ | 245mH/80Ω | 255mH/80Ω |
| 4 | (Simulation) | | |
| | ($L_{d1}/R_{d1}$) | 50mH/10Ω | 50mH/10Ω |
| | ($L_{d2}/R_{d2}$) | No | 70mH/30Ω |
| | (Experiment) | | |
| | ($L_{d1}/R_{d1}$) | 70mH/10Ω | 120mH/20Ω |
| | ($L_{d2}/R_{d2}$) | No | 150mH/67Ω |
| 5 | $L_{f1}/C_{f1}$ | 1.5mH/25μF | 1.8mH/25μF |
| | $L_{f2}/C_{f2}$ | 1.5mH/25μF | 1.5mH/50μF |
| 6 | $L_{c1}/R_{c1}$ | 1.8mH/0.2Ω | 2.3mH/0.4Ω |
| | $L_{c2}/R_{c2}$ | 1.8mH/0.2Ω | 2.1mH/0.4Ω |

the rejection capability for multiple disturbances occurrence. The case5 investigates robustness for LC filters parameters perturbation. The case6 investigates robustness for output impedances perturbation of inverters. The case7 validates voltage disturbance rejection ability in the presence of DG unit fault. The key parameters of configuration and controller in the case setup are given in Table I. And the perturbation parameters for robustness investigation are reported in Table Ⅱ.

### A. Case1: The proposed estimator-based control strategy.

In the setup analyzed, the control objective of proposed voltage controller is to hold bus3 voltage to track its steady-state set point. Hence, bus3 weighting coefficient $w_{b3}$ in voltage controller is set to 1000 and others are set to 0.1, which means voltage control for bus 3 has a top priority while others are neglected due to the much smaller weighting coefficients.

To validate the proposed control strategy, disturbance load1 ($L_{d1}/R_{d1}$) is exerted at bus 2, shown in Fig. 11. It can be seen from Fig. 13(a)-(c) that bus voltages drop (black curves) since droop controller decreases voltage to track the increased reactive power. Further, once the proposed voltage control strategy is activated, the bus3 voltage is brought to original value as shown in Fig. 13(c). And other buses, of course, appear the steady-state offset due to smaller weighting coefficients (green curves).

Also, in the corresponding experiment, disturbance load1 ($L_{d1}/R_{d1}$) is exerted at bus2. The voltage responses obtained from the experimental setup are depicted in Fig. 13(d)-(f). The experiment results show that the proposed controller drives bus3 voltage to original value accurately once voltage drops. One can note the tight correspondence between the simulated and experimental results. The correctness and reliability of the proposed control strategy thus is confirmed.

### B. Case2: The robustness Investigation for line parameter perturbation

To verify robustness of the voltage controller for line parameters perturbation, line parameters are changed intentionally as shown in TableⅡ. Meanwhile, disturbance load1 is exerted at bus2. Fig. 14(a)-(c) depicts bus voltage responses under line parameters perturbation when load disturbance occurs (black curves), where up to 12V and 9V voltages drops at bus2 and bus3 respectively. In the case, the control objective of controller is still forcing bus3 voltage return to original value. With respect to Fig. 14(c), an about 0.3V steady-state error appears when line parameters perturbations occur, but voltage control behavior is still desirable and satisfied. To further validate robustness of the voltage controller, the further experiments are implemented, where disturbance load1 ($L_{d1}/R_{d1}$) is exerted at bus2. The experimental results about line parameters perturbations are shown in Fig. 14(f). It can be seen that bus3 voltage is brought to original state even if line parameter is perturbed.

### C. Case3: The robustness Investigation for load parameters variation

The loads parameters perturbation is also a leading factor that affects the robustness of the voltage controller since loads parameters are also introduced to the discrete time model aforementioned. The simulation and experimental results for loads parameters variation are shown in Fig. 15.

Fig. 15(c) and Fig. 15(f) show that the proposed controller is able to drive bus3 voltage back to original set point accurately, even if all the load parameters are perturbed intentionally within a neighbor range of steady-state values.

### D. Case4: The robustness verification for different disturbance locations.

The case4 is to investigate rejection ability of the voltage controller to unknown multiple disturbances, which was not considered in the design of original controller yet. As described in Section Ⅲ. B, the rejection capability for unknown disturbances can be achieved by internal model augmentation. In the case, disturbance load2 ($L_{d2}/R_{d2}$) along with disturbance load1, is imposed to exert at bus 2 and 3 respectively as shown in Fig. 11, and voltage restoration for bus3 is still only control objective. As it can be seen in Fig. 16(a)-(c), multiple disturbances lead to up to 15V and 13V voltages droop at bus2 and bus3 respectively.

This article has been accepted for publication in a future issue of this journal, but has not been fully edited. Content may change prior to final publication. Citation information: DOI 10.1109/TPEL.2014.2345696, IEEE Transactions on Power Electronics





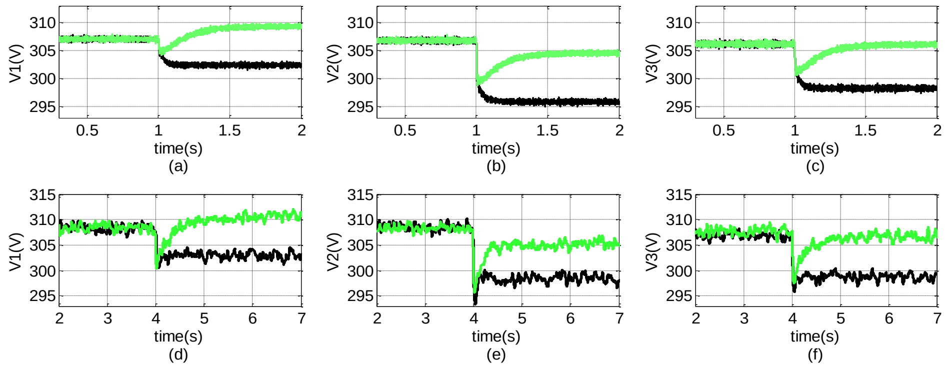


Fig. 13. The simulation and experimental results of voltage responses under load disturbance with (green curves) and without (black curves) the proposed control method.

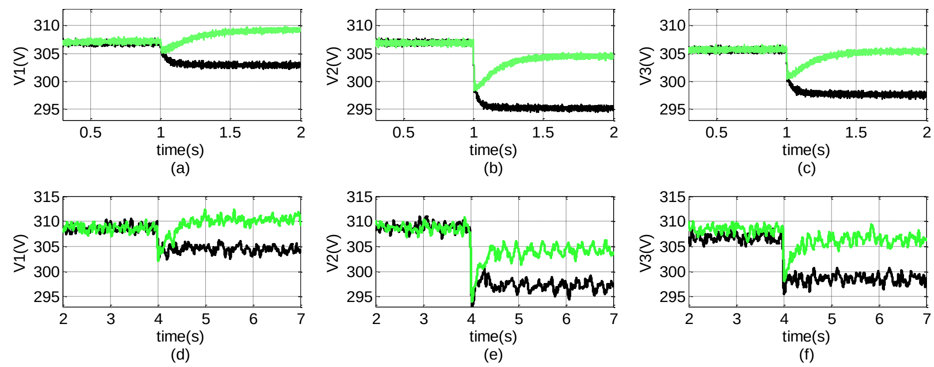


Fig. 14. The simulation and experimental results for robustness to line parameters perturbations with (green curves) and without (black curves) the proposed control strategy.

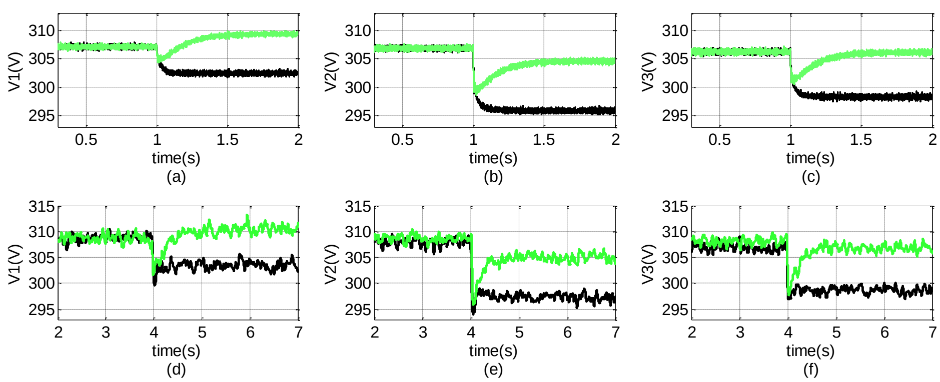


Fig. 15. The simulation and experimental results for robustness to load parameter perturbation with (green curves) and without (black curves) the proposed control strategy.

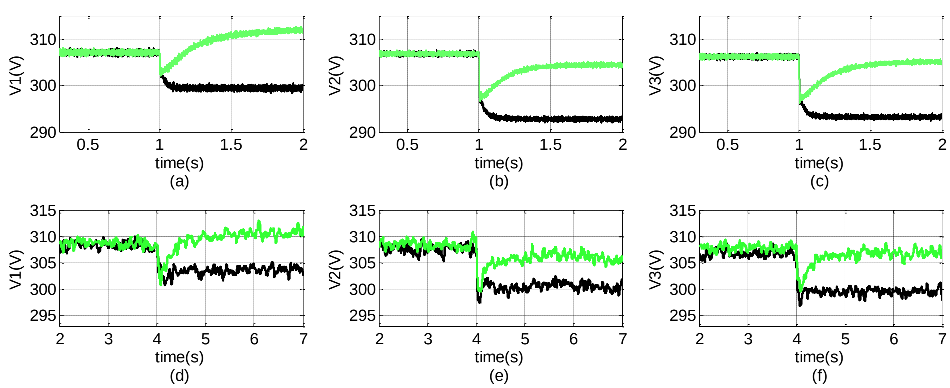


Fig. 16. The simulation and experimental results for different disturbance positions with (green curves) and without (black curves) the proposed control strategy.

This article has been accepted for publication in a future issue of this journal, but has not been fully edited. Content may change prior to final publication. Citation information: DOI 10.1109/TPEL.2014.2345696, IEEE Transactions on Power Electronics





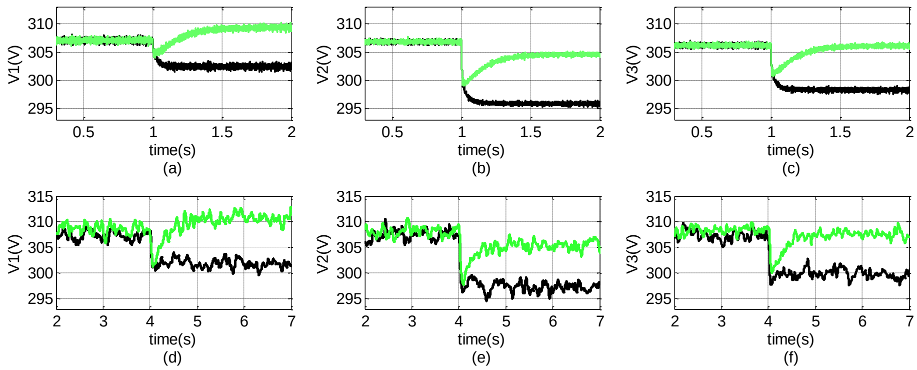


Fig. 17. The simulation and experimental results for robustness to LC filters perturbations with (green curves) and without (black curves) the proposed control strategy.

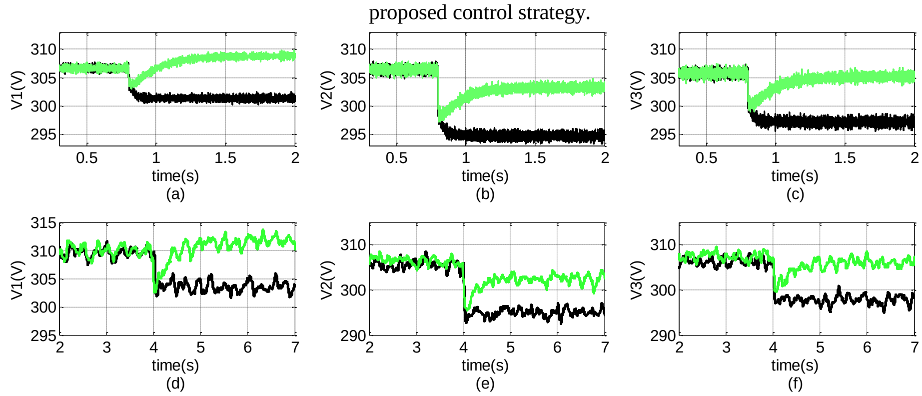


Fig. 18. The simulation and experimental results for robustness to output impedance perturbations with (green curves) and without (black curves) the proposed control strategy.

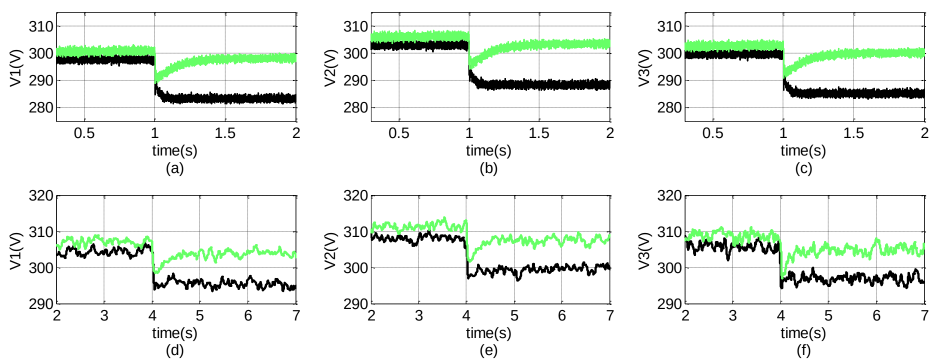


Fig. 19. The simulation and experimental results for robustness to DG unit fault with (green curves) and without (black curves) the proposed control strategy.

When the proposed voltage controller is activated,bus3 voltage rises towards original value even if a slight offset occurs, which is within 3% of the voltage droop maximum as shown in Fig. 16(c).

The case shows that the proposed controller is still valid when multiple disturbances appear at different buses. The experimental results reported in Fig. 16(d)-(f), along with the simulation results, point out that the proposed voltage predictive controller has a good capability to reject unknown multiple disturbances.

### *E. Case5: The robustness investigation for LC filters perturbation*

The case5 investigates the robustness for LC filters perturbation, where LC filters parameters are perturbed intentionally as shown in Table II. In simulation, disturbance load1 ($L_{d1}$/$R_{d1}$) appears at bus2. It can be seen that voltages drop at different buses (black curves) as shown in Fig. 17(a)-(c). Also, Fig. 17(d)-(f) reports the voltage responses (black curves) from experimental implementation in the presence of the disturbance load1. The voltage controller is still planned to bring bus3 voltage back to original state. Fig. 17(c) and Fig. 17(f) illustrate that the proposed voltage controller is able to perform voltage restoration at bus3 even if LC filters parameters are perturbed. Therefore, the simulation and experimental results point out that the proposed voltage controller has a good robustness against LC filters perturbations.

### *F. Case6: The robustness investigation for output impedances perturbation*

In addition, the output impedance $L_c$ of inverters maybe has a significant influence on the robustness of the voltage controller. Hence, the case6 is carried out in order to validate

This article has been accepted for publication in a future issue of this journal, but has not been fully edited. Content may change prior to final publication. Citation information: DOI 10.1109/TPEL.2014.2345696, IEEE Transactions on Power Electronics





controller performance under output impedances perturbation. The output impedances of inverters are changed intentionally as shown in TableII. In the implementation of simulation and experiment, the disturbance load1 is exerted at bus2. The voltages response (black curves) can be observed in Fig. 18.

It can be seen from Fig. 18(a)-(c) and Fig. 18(d)-(f) that the proposed voltage controller is able to force bus3 voltage return to original value when voltages drop (green curves). Thus the results obtained from simulations and experiments validate robustness under output impedance perturbations.

### *G. Case7: The robustness investigation for DG unit fault.*

To validate robustness of the proposed voltage controller in the presence of DG unit fault, the set of simulations and experiments is performed. With the assumption that DG unit1 fault happens suddenly and disconnects from the system, disturbance load1 ($L_{d1}/R_{d1}$) is exerted at bus2. Then DG unit2 is just responsible for control system voltages, since DG1 losses the contribution to control voltage. As it can be seen in Fig. 19, the disturbance results in up to 14V and 15V voltages droop at bus2 and bus3 respectively (black curves). The control objective is still to hold bus3 voltage at its original state. With respect to Fig. 19(c), an about 1.2V control offset appears in the presence of DG unit1 fault. But the control result is still desirable and accepted.

Similarly, in the accompanying experiment, the DG unit1 is disconnected suddenly from the system setup. And the disturbance load (70mH/20Ω) occurs at bus2. Then the voltage controller of DG unit2 is just responsible for voltage restoration within the whole system. The experimental results depicted in Fig. 19(d)-(f), together with the simulation results, point out that the proposed voltage controller is still able to perform bus3 voltage restoration even if a about 1V voltage offset occurs under DG unit1 fault. Hence, the case validates the robustness of the proposed controller under DG unit fault.

## Ⅶ. CONCLUSION

In this paper, an estimator-based voltage predictive control strategy for AC islanded microgrids has been proposed. First, a network voltage estimator associated with each DG unit has been proposed to obtain voltages response without communication links. Second, a voltage predictive controller with immunity to parameters perturbation has been developed to implement the offset-free voltage control for the specified bus. Furthermore, the dynamic performance of the proposed controller was analyzed through small signal analysis method. The analysis results show that voltage error weighting coefficient and voltage control input increment weighting coefficient have a dramatic influence on system dynamic performance. Finally, robustness of the proposed voltage controller was investigated under system parameters uncertainties. The investigation results from simulations and experiments show that the proposed estimator-based voltage control strategy is able to implement offset-free voltage control for the specified bus in an AC islanded microgrid, and has a good capability to reject uncertain parameters perturbations. The proposed voltage control strategy can be implemented easily without communication facilities and thus improve flexibility and reliability of islanded microgrids.

## APPENDIX

TABLE 1
Initial Conditions

| Parameter | Value | Parameter | Value |
|---|---|---|---|
| $\delta_{i0}$ | [0,0.02] | $\omega_{i0}$ | [313.9,313.9] |
| $I_{odi0}$ | [6.4,1.6] | $I_{oqi0}$ | [2.7,3.9] |
| $V_{odi0}$ | [309.87,309.32] | $V_{oqi0}$ | [0,0] |
| $V_{bDi0}$ | [307.06,306.73,306.15] | $V_{bQi0}$ | [3.08,6.28,4.6] |
| $I_{Linedi0}$ | [3.4,-1.45] | $I_{Lineqi0}$ | [3.87,1.56] |

The small signal model of an individual inverter in d-q frame can be transferred to common D-Q frame [2] as follow:

$$\Delta i_{oDQi} = T_{1i}\Delta i_{odqi} + T_{2i}\Delta\delta_i \quad \Delta V_{bdqi} = T_{3i}\Delta V_{bDQi} + T_{4i}\Delta\delta_i$$

$$T_{1i} = \begin{bmatrix} \cos(\delta_{i0}) & -\sin(\delta_{i0}) \\ \sin(\delta_{i0}) & \cos(\delta_{i0}) \end{bmatrix} T_{3i} = \begin{bmatrix} \cos(\delta_{i0}) & \sin(\delta_{i0}) \\ -\sin(\delta_{i0}) & \cos(\delta_{i0}) \end{bmatrix}$$

$$T_{2i} = \begin{bmatrix} -I_{odi0}\sin(\delta_{i0}) - I_{oqi0}\cos(\delta_{i0}) \\ I_{odi0}\cos(\delta_{i0}) - I_{oqi0}\sin(\delta_{i0}) \end{bmatrix}, \quad A_{curi1} = \begin{bmatrix} -I_{oqi0} \\ I_{odi0} \end{bmatrix}_{6\times2}$$

$$T_{4i} = \begin{bmatrix} -V_{bDi0}\sin(\delta_{i0}) + V_{bQi0}\cos(\delta_{i0}) \\ -V_{bDi0}\cos(\delta_{i0}) - V_{bQi0}\sin(\delta_{i0}) \end{bmatrix}.$$

$$A_{curi2} = \begin{bmatrix} \frac{1}{L_c} & 0 \\ 0 & \frac{1}{L_c} \end{bmatrix}, \quad A_{curi3} = \begin{bmatrix} -\frac{R_c}{L_c} & -\omega_{i0} \\ \omega_{i0} & \frac{R_c}{L_c} \end{bmatrix} (i=1,2) \; B_{curi} = \begin{bmatrix} -\frac{1}{L_c} & 0 \\ 0 & -\frac{1}{L_c} \end{bmatrix},$$

$$A_{inv} = \begin{bmatrix} A_{inv1t} & O_{6\times6} \\ T_{pm1} & A_{inv2t} \end{bmatrix}, \quad B_{inv} = \begin{bmatrix} B_{inv1} & O & O \\ O & B_{inv2}T_{32} & O \end{bmatrix}, \quad A_{inv1t} = A_{inv1} + B_{inv1}T_{V1},$$

$$T_{V1} = T_{41}[1,0,0,0,0,0], \quad T_{pm1} = \begin{bmatrix} O & -m_{p1} & O \\ O & \cdots & O \end{bmatrix}, \quad A_{inv2t} = A_{inv2} + B_{inv2}T_{V2},$$

$$T_{V2} = T_{42}[1,0,0,0,0,0], \quad A_{invi} = \begin{bmatrix} O & A_1 & O & O \\ O & A_2 & A_3 & A_4 \\ O & O & A_5 & A_6 \\ O & L_1 & L_2 & L_3 \end{bmatrix}_{6\times6} \quad (i=1,2)$$

$$B_{invi} = \begin{bmatrix} O \\ L_4 \end{bmatrix}_{6\times2} \quad (i=1,2), \; A_1 = m_{pi}(i=1,2), \; A_2 = \begin{bmatrix} -\omega_c & 0 \\ 0 & -\omega_c \end{bmatrix},$$

$$A_3 = \begin{bmatrix} \omega_c i_{odi0} \\ \omega_c i_{oqi0} \end{bmatrix} (i=1,2), \; A_4 = \begin{bmatrix} \omega_c V_{odi0} & \omega_c V_{oqi0} \\ -\omega_c V_{oqi0} & \omega_c V_{odi0} \end{bmatrix},$$

$$A_5 = -\omega_c - n_{qi}\omega_c i_{oqi0}, \; A_6 = \begin{bmatrix} n_{qi}\omega_c V_{oqi0} & -n_{qi}\omega_c V_{odi0} \end{bmatrix},$$

$$L_1 = \begin{bmatrix} m_p i_{oqi0} \\ -m_p i_{odi0} \end{bmatrix} (i=1,2), \; L_2 = \begin{bmatrix} \frac{1}{L_c} \\ 0 \end{bmatrix}, \; L_2 = \begin{bmatrix} \frac{1}{L_c} & 0 \\ 0 & \frac{1}{L_c} \end{bmatrix}, \quad T_{invi} = [T_{2i}, O, T_{1i}],$$

$$\Delta i_{oDQi} = T_{inv}\Delta x_{invi} \; A_{Line} = \begin{bmatrix} L_{110} & L_{120} \\ L_{210} & L_{220} \end{bmatrix}, \; B_{Line1} = \begin{bmatrix} L_{130} & L_{140} \\ L_{230} & L_{240} \end{bmatrix},$$

$$B_{Line2} = \begin{bmatrix} L_{150} & L_{160} \\ L_{250} & L_{260} \end{bmatrix}, \; B_{Line3} = \begin{bmatrix} L_{170} \\ L_{270} \end{bmatrix}, \; B_{dis} = \begin{bmatrix} B_{r1} \\ B_{r2} \end{bmatrix}, \; L_{110} = \begin{bmatrix} L_{11} & -\omega_{10} \\ \omega_{10} & L_{11} \end{bmatrix},$$

$$L_{120} = \begin{bmatrix} L_{12} & 0 \\ 0 & L_{12} \end{bmatrix}, \; L_{130} = \begin{bmatrix} L_{13} & L_{15}\omega_{10} \\ -L_{15}\omega_{10} & L_{13} \end{bmatrix}, \; L_{140} = \begin{bmatrix} L_{14} & L_{16}\omega_{10} \\ -L_{16}\omega_{10} & L_{14} \end{bmatrix},$$

This article has been accepted for publication in a future issue of this journal, but has not been fully edited. Content may change prior to final publication. Citation information: DOI 10.1109/TPEL.2014.2345696, IEEE Transactions on Power Electronics


$$L_{150}=\begin{bmatrix}L_{15} & 0\\ 0 & L_{15}\end{bmatrix}, L_{160}=\begin{bmatrix}L_{16} & 0\\ 0 & L_{16}\end{bmatrix},$$

$$L_{170}=\begin{bmatrix}-I_{Lineq10}+L_{15}I_{oq10}+L_{16}I_{oq20}\\ I_{Lined10}-L_{15}I_{od10}-L_{16}I_{od20}\end{bmatrix}\quad L_{210}=\begin{bmatrix}L_{21} & 0\\ 0 & L_{21}\end{bmatrix},$$

$$L_{220}=\begin{bmatrix}L_{22} & -\omega_{10}\\ \omega_{10} & L_{22}\end{bmatrix},\qquad L_{230}=\begin{bmatrix}L_{23} & L_{25}\omega_{10}\\ -L_{25}\omega_{10} & L_{23}\end{bmatrix},$$

$$L_{240}=\begin{bmatrix}L_{24} & L_{26}\omega_{10}\\ -L_{26}\omega_{10} & L_{24}\end{bmatrix}, L_{250}=\begin{bmatrix}L_{25} & 0\\ 0 & L_{25}\end{bmatrix}, L_{260}=\begin{bmatrix}L_{26} & 0\\ 0 & L_{26}\end{bmatrix},$$

$$L_{270}=\begin{bmatrix}-I_{Lineq20}+L_{25}I_{oq10}+L_{26}I_{oq20}\\ I_{Lined20}-L_{25}I_{od10}-L_{26}I_{od20}\end{bmatrix}$$

$$L_{11}=-\frac{(1+\frac{L_{Load2}}{L_2}+\frac{L_{Load3}}{L_2})(\frac{R_1}{L_1}+\frac{R_{Load1}}{L_1}+\frac{R_{Load3}}{L_1})-\frac{L_{Load3}R_{Load3}}{L_1L_2}}{(\frac{L_{Load1}}{L_1}+\frac{L_{Load3}}{L_1}+1)(\frac{L_{Load2}}{L_2}+\frac{L_{Load3}}{L_2}+1)-\frac{L_{Load3}^2}{L_1L_2}}$$

$$L_{12}=-\frac{\frac{R_{Load3}(\frac{L_{Load2}}{L_2}+\frac{L_{Load3}}{L_2}+1)}{L_1}-\frac{L_{Load1}(\frac{R_2}{L_2}+\frac{R_{Load2}}{L_2}+\frac{R_{Load3}}{L_2})}{L_1}}{(\frac{L_{Load1}}{L_1}+\frac{L_{Load3}}{L_1}+1)(\frac{L_{Load2}}{L_2}+\frac{L_{Load3}}{L_2}+1)-\frac{L_{Load3}^2}{L_1L_2}}$$

$$L_{13}=\frac{\frac{R_{Load1}(\frac{L_{Load2}}{L_2}+\frac{L_{Load3}}{L_2}+1)}{L_1}}{(\frac{L_{Load1}}{L_1}+\frac{L_{Load3}}{L_1}+1)(\frac{L_{Load2}}{L_2}+\frac{L_{Load3}}{L_2}+1)-\frac{L_{Load3}^2}{L_1L_2}}$$

$$L_{14}=-\frac{\frac{R_{Load2}L_{Load3}}{L_1L_2}}{(\frac{L_{Load1}}{L_1}+\frac{L_{Load3}}{L_1}+1)(\frac{L_{Load2}}{L_2}+\frac{L_{Load3}}{L_2}+1)-\frac{L_{Load3}^2}{L_1L_2}}$$

$$L_{15}=\frac{\frac{L_{Load1}(\frac{L_{Load2}}{L_2}+\frac{L_{Load3}}{L_2}+1)}{L_1}}{(\frac{L_{Load1}}{L_1}+\frac{L_{Load3}}{L_1}+1)(\frac{L_{Load2}}{L_2}+\frac{L_{Load3}}{L_2}+1)-\frac{L_{Load3}^2}{L_1L_2}}$$

$$L_{16}=-\frac{\frac{L_{Load2}L_{Load3}}{L_1L_2}}{(\frac{L_{Load1}}{L_1}+\frac{L_{Load3}}{L_1}+1)(\frac{L_{Load2}}{L_2}+\frac{L_{Load3}}{L_2}+1)-\frac{L_{Load3}^2}{L_1L_2}}$$

$$L_{21}=-\frac{\frac{R_{Load3}(\frac{L_{Load1}}{L_1}+\frac{L_{Load3}}{L_1}+1)}{L_2}-\frac{L_{Load3}(\frac{R_1}{L_1}+\frac{R_{Load1}}{L_1}+\frac{R_{Load3}}{L_1})}{L_2}}{(\frac{L_{Load1}}{L_1}+\frac{L_{Load3}}{L_1}+1)(\frac{L_{Load2}}{L_2}+\frac{L_{Load3}}{L_2}+1)-\frac{L_{Load3}^2}{L_1L_2}}$$

$$L_{22}=-\frac{(1+\frac{L_{Load1}}{L_1}+\frac{L_{Load3}}{L_1})(\frac{R_2}{L_2}+\frac{R_{Load2}}{L_2}+\frac{R_{Load3}}{L_2})-\frac{L_{Load3}R_{Load3}}{L_1L_2}}{(\frac{L_{Load1}}{L_1}+\frac{L_{Load3}}{L_1}+1)(\frac{L_{Load2}}{L_2}+\frac{L_{Load3}}{L_2}+1)-\frac{L_{Load3}^2}{L_1L_2}}$$

$$L_{23}=-\frac{\frac{L_{Load3}}{L_1L_2R_{Load1}}}{(\frac{L_{Load1}}{L_1}+\frac{L_{Load3}}{L_1}+1)(\frac{L_{Load2}}{L_2}+\frac{L_{Load3}}{L_2}+1)-\frac{L_{Load3}^2}{L_1L_2}}$$

$$L_{25}=-\frac{\frac{L_{Load1}L_{Load3}}{L_1L_2}}{(\frac{L_{Load1}}{L_1}+\frac{L_{Load3}}{L_1}+1)(\frac{L_{Load2}}{L_2}+\frac{L_{Load3}}{L_2}+1)-\frac{L_{Load3}^2}{L_1L_2}}$$

$$L_{24}=\frac{\frac{R_{Load2}(\frac{L_{Load1}}{L_1}+\frac{L_{Load3}}{L_1}+1)}{L_2}}{(\frac{L_{Load1}}{L_1}+\frac{L_{Load3}}{L_1}+1)(\frac{L_{Load2}}{L_2}+\frac{L_{Load3}}{L_2}+1)-\frac{L_{Load3}^2}{L_1L_2}}$$

$$L_{26}=\frac{\frac{L_{Load2}(\frac{L_{Load1}}{L_1}+\frac{L_{Load3}}{L_1}+1)}{L_2}}{(\frac{L_{Load1}}{L_1}+\frac{L_{Load3}}{L_1}+1)(\frac{L_{Load2}}{L_2}+\frac{L_{Load3}}{L_2}+1)-\frac{L_{Load3}^2}{L_1L_2}}$$

$$A_{Load}=\begin{bmatrix}h_{41} & O & O\\ O & h_{42} & O\\ O & O & h_{43}\end{bmatrix}, B_{Load1}=\begin{bmatrix}h_{21} & h_{31}\\ h_{22} & h_{32}\\ h_{23} & h_{33}\end{bmatrix}, B_{Load2}=\begin{bmatrix}h_{51} & h_{61}\\ h_{52} & h_{62}\\ h_{53} & h_{63}\end{bmatrix},$$

$$B_{Load3}=\begin{bmatrix}h_{71} & h_{81}\\ h_{72} & h_{82}\\ h_{73} & h_{83}\end{bmatrix}, B_{Load4}=\begin{bmatrix}h_{11}\\ h_{12}\\ h_{13}\end{bmatrix}, B_{dis2}=\begin{bmatrix}h_{91}\\ h_{92}\\ h_{93}\end{bmatrix}; h_{11}=L_{f5}+L_{f4}L_{170},$$

$$h_{21}=L_{f1}+L_{f4}L_{110}, h_{31}=L_{f4}L_{120}, h_{41}=L_{f1}, h_{51}=L_{f2}+L_{f4}L_{130}$$

$$h_{61}=L_{f4}L_{140}, h_{71}=L_{f3}+L_{f4}L_{150}, h_{81}=L_{f4}L_{160}, h_{91}=L_{f4}B_{r1}$$

$$L_{f1}=\begin{bmatrix}-\frac{R_{Load1}}{L_{Load1}} & -\omega_{10}\\ \omega_{10} & -\frac{R_{Load1}}{L_{Load1}}\end{bmatrix}, L_{f2}=\begin{bmatrix}\frac{R_{Load1}}{L_{Load1}} & \omega_{10}\\ -\omega_{10} & \frac{R_{Load1}}{L_{Load1}}\end{bmatrix}, L_{f3}=\begin{bmatrix}1 & 0\\ 0 & 1\end{bmatrix},$$

$$L_{f4}=\begin{bmatrix}-1 & 0\\ 0 & -1\end{bmatrix}\qquad L_{f5}=\begin{bmatrix}-I_{Loadq10}+I_{oq10}-I_{Lineq10}\\ I_{Loadd10}-I_{od10}+I_{Lined10}\end{bmatrix}.$$

$$h_{12}=L_{f52}+L_{f42}L_{270}, h_{22}=L_{f42}L_{210}, h_{32}=L_{f12}+L_{f42}L_{220},$$

$$h_{42}=L_{f12}, h_{52}=L_{f42}L_{230}, h_{62}=L_{f22}+L_{f42}L_{240}, h_{72}=L_{f42}L_{250},$$

$$h_{82}=L_{f32}+L_{f42}L_{260}, h_{92}=L_{f42}B_{r2}+L_{f22}$$

$$L_{f12}=\begin{bmatrix}-\frac{R_{Load2}}{L_{Load2}} & -\omega_{10}\\ \omega_{10} & -\frac{R_{Load2}}{L_{Load2}}\end{bmatrix},\qquad L_{f22}=\begin{bmatrix}\frac{R_{Load2}}{L_{Load2}} & \omega_{10}\\ -\omega_{10} & \frac{R_{Load2}}{L_{Load2}}\end{bmatrix},$$

$$L_{f32}=\begin{bmatrix}1 & 0\\ 0 & 1\end{bmatrix}, L_{f42}=\begin{bmatrix}-1 & 0\\ 0 & -1\end{bmatrix}\quad L_{f52}=\begin{bmatrix}-I_{Loadq20}+I_{oq20}-I_{Lineq20}\\ I_{Loadd20}-I_{od20}+I_{Lined20}\end{bmatrix}$$

$$h_{13}=L_{f43}+L_{f33}L_{170}+L_{f33}L_{270},\quad h_{23}=L_{f13}+L_{f33}L_{110}+L_{f33}L_{210},$$

$$h_{33}=L_{f13}+L_{f33}L_{120}+L_{f33}L_{220}\qquad h_{43}=L_{f23},$$

$$h_{53}=L_{f33}L_{130}+L_{f33}L_{230},\quad h_{63}=L_{f33}L_{140}+L_{f33}L_{240},$$

$$h_{73}=L_{f33}L_{150}+L_{f33}L_{250},\quad h_{83}=L_{f33}L_{160}+L_{f33}L_{260},$$

$$h_{93}=L_{f33}B_{r1}+L_{f33}B_{r2}\quad L_{f13}=\begin{bmatrix}\frac{R_{Load3}}{L_{Load3}} & \omega_{10}\\ -\omega_{10} & \frac{R_{Load3}}{L_{Load3}}\end{bmatrix}, L_{f33}=\begin{bmatrix}1 & 0\\ 0 & 1\end{bmatrix}$$

$$L_{f23}=\begin{bmatrix}-\frac{R_{Load3}}{L_{Load3}} & -\omega_{10}\\ \omega_{10} & -\frac{R_{Load3}}{L_{Load3}}\end{bmatrix}, L_{f43}=\begin{bmatrix}-I_{Loadq30}+I_{Lineq10}+I_{Lineq20}\\ I_{Loadd30}-I_{Lined10}-I_{Lined20}\end{bmatrix}$$

Network model parameters:

$$A_{net}=\begin{bmatrix}A_{Line} & O\\ B_{Load1} & A_{Load}\end{bmatrix}, B_{net1}=\begin{bmatrix}B_{Line1}\\ B_{Load2}\end{bmatrix}, B_{net2}=\begin{bmatrix}B_{Line2}\\ B_{Load3}\end{bmatrix},$$

$$B_{net3}=\begin{bmatrix}B_{Line3}\\ B_{Load4}\end{bmatrix}, B_{net4}=\begin{bmatrix}B_{dis}\\ B_{dis2}\end{bmatrix}$$

This article has been accepted for publication in a future issue of this journal, but has not been fully edited. Content may change prior to final publication. Citation information: DOI 10.1109/TPEL.2014.2345696, IEEE Transactions on Power Electronics



Bus voltages parameters:

$$C_{vol}=F_4T_w+F_2T_{inv}+F_3T_{inv}A_{s1},\quad C_{vol2}=F_1+F_3T_{inv}A_{s2},$$

$$D=F_3T_{inv}B_{s1}+F_5$$

$$F_1=\begin{bmatrix}V_{f41} & V_{f51} & O\\ V_{f42} & V_{f52} & \vdots\\ V_{f43} & V_{f53} & O\end{bmatrix},\quad F_2=\begin{bmatrix}V_{f21} & V_{f31}\\ V_{f22} & V_{f32}\\ V_{f23} & V_{f33}\end{bmatrix},\quad F_3=\begin{bmatrix}V_{f61} & V_{f71}\\ V_{f62} & V_{f72}\\ V_{f63} & V_{f73}\end{bmatrix},$$

$$F_4=\begin{bmatrix}V_{f11}\\ V_{f12}\\ V_{f13}\end{bmatrix},\qquad F_5=\begin{bmatrix}V_{f81}\\ V_{f82}\\ V_{f83}\end{bmatrix},V_{11}=\begin{bmatrix}R_{Load1} & L_{Load1}\omega_{10}\\ -L_{Load1}\omega_{10} & R_{Load1}\end{bmatrix}$$

$$V_{f11}=V_{51}+V_{41}L_{170},V_{f21}=V_{11}+V_{41}L_{130},V_{f31}=V_{41}L_{140},$$

$$V_{f41}=V_{21}+V_{41}L_{110},V_{f51}=V_{41}L_{120},V_{f61}=V_{31}+V_{41}L_{150},$$

$$V_{f71}=V_{41}L_{160},\ V_{f81}=V_{41}B_{r1},$$

$$,V_{21}=\begin{bmatrix}-R_{Load1} & -L_{Load1}\omega_{10}\\ L_{Load1}\omega_{10} & -R_{Load1}\end{bmatrix},V_{31}=\begin{bmatrix}L_{Load1} & 0\\ 0 & L_{Load1}\end{bmatrix},$$

$$V_{41}=\begin{bmatrix}-L_{Load1} & 0\\ 0 & -L_{Load1}\end{bmatrix},\ V_{51}=\begin{bmatrix}L_{Load1}I_{oq10}-L_{Load1}I_{Lineq10}\\ -L_{Load1}I_{od10}+L_{Load1}I_{Lined10}\end{bmatrix},$$

$$V_{f12}=V_{52}+V_{42}L_{270},V_{f22}=V_{42}L_{230},V_{f32}=V_{12}+V_{42}L_{240},$$

$$V_{f42}=V_{42}L_{210},V_{f52}=V_{22}+V_{42}L_{220},V_{f62}=V_{42}L_{250},$$

$$V_{f72}=V_{32}+V_{42}L_{260},$$

$$V_{f82}=V_{42}B_{r2}+V_{B2};V_{12}=\begin{bmatrix}R_{Load2} & L_{Load2}\omega_{20}\\ -L_{Load2}\omega_{20} & R_{Load2}\end{bmatrix},$$

$$V_{22}=\begin{bmatrix}-R_{Load2} & -L_{Load2}\omega_{20}\\ L_{Load2}\omega_{20} & -R_{Load2}\end{bmatrix},\quad V_{32}=\begin{bmatrix}L_{Load2} & 0\\ 0 & L_{Load2}\end{bmatrix}$$

$$V_{42}=\begin{bmatrix}-L_{Load2} & 0\\ 0 & -L_{Load2}\end{bmatrix},V_{B2}=\begin{bmatrix}R_{Load2} & L_{Load2}\omega_{10}\\ -L_{Load2}\omega_{10} & R_{Load2}\end{bmatrix}$$

$$V_{52}=\begin{bmatrix}L_{Load2}I_{oq20}-L_{Load2}I_{Lineq20}+L_{Load2}I_{disq0}\\ -L_{Load2}I_{od20}+L_{Load2}I_{Lined20}-L_{Load2}I_{disd0}\end{bmatrix}$$

$$V_{f13}=V_{33}+V_{23}L_{170}+V_{23}L_{270},V_{f23}=V_{23}L_{130}+V_{23}L_{230},$$

$$V_{f33}=V_{23}L_{140}+V_{23}L_{240},V_{f43}=V_{13}+V_{23}L_{110}+V_{23}L_{210},$$

$$V_{f53}=V_{13}+V_{23}L_{120}+V_{23}L_{220},V_{f63}=V_{23}L_{150}+V_{23}L_{250},$$

$$V_{f73}=V_{23}L_{160}+V_{23}L_{260},V_{f83}=V_{23}B_{r1}+V_{23}B_{r2}$$

$$V_{13}=\begin{bmatrix}R_{Load3} & L_{Load3}\omega_{10}\\ -L_{Load3}\omega_{10} & R_{Load3}\end{bmatrix},V_{23}=\begin{bmatrix}L_{Load3} & 0\\ 0 & L_{Load3}\end{bmatrix},$$

$$V_{33}=\begin{bmatrix}L_{Load3}I_{Lineq10}+L_{Load3}I_{Lineq20}\\ -L_{Load3}I_{Lined10}-L_{Load3}I_{Lined20}\end{bmatrix}$$

$$A_{s1}=\left(I-B_{inv}F_3T_{inv}\right)^{-1}\left(A_{inv}+B_{inv}F_2T_{inv}+B_{inv}F_4T_w\right);$$

$$A_{s2}=\left(I-B_{inv}F_3T_{inv}\right)^{-1}B_{inv}F_1\quad A_{s3}=G_3T_{inv}A_{s1}+G_2T_{inv}+G_4T_w,$$

$$A_{s4}=G_1+G_3T_{inv}A_{s2},B_{s1}=\left(I-B_{inv}F_3T_{inv}\right)^{-1}B_{inv}F_5$$

$$A=\begin{bmatrix}A_{s1} & A_{s2}\\ A_{s3} & A_{s4}\end{bmatrix},\quad B=\begin{bmatrix}B_{s1}\\ G_6\end{bmatrix},\quad C=\begin{bmatrix}F_{o1} & F_{o2}\end{bmatrix},D=F_{o3}.$$

## REFERENCES


[1] R. H. Lasseter, ‘‘Smart distribution: Coupled microgrids,’’ *Proc. IEEE*, vol. 99, no. 6, pp. 1074-1082, Jun. 2011.

[2] N. Pogaku, M. Prodanovic, and T. C. Green, “Modeling, analysis and testing of autonomous operation of an inverter-based microgrid,” *IEEE Trans. Power Electron*., vol. 22, no. 2, pp. 613-625, Mar. 2007.

[3] E. Mashhour, and S. M. Moghaddas-Tafreshi, “Bidding strategy of virtual power plant for participating in energy and spinning reserve markets – Part Ⅰ: problem formulation,” *IEEE Trans. power syst.*, vol. 26, no. 2, pp. 949-956, May. 2011.

[4] Y. Abdel-Rady, I. Mohamed, and E. F. El-Saadany, “Adaptive decentralized droop controller to preserve power sharing stability of paralleled inverters in distributed generation microgrids,” *IEEE Trans. Power Electron.*, vol. 23, no. 6, pp. 2806-2816, Nov. 2008.

[5] C. L. Chen, Y. Wang, J. S. Lai, Y-S. Lee, and D. Martin, “Design of parallel inverters for smooth mode transfer microgrid applications,” *IEEE Trans. Power Electron.*, vol. 25, no. 1, pp. 6-15, Jan. 2010.

[6] Y. W. Li, and C. N. Kao, “An accurate power control strategy for power-electronics-interfaced distributed generation units operating in a low-voltage multibus microgrid,” *IEEE Trans. Power Electron.*, vol. 24, no. 12, pp. 2977-2988, Dec. 2009.

[7] Q. C. Zhong, “Robust droop controller for accurate proportional load sharing among inverters operated in parallel,” *IEEE Trans. Ind. Electron.*, vol. 60, no. 4, pp. 1281-1290, Apr. 2013.

[8] J. W. He, Y. W. Li, J. M. Guerrero, F. Blaabjerg, and J. C. Vasquez, “An islanding microgrid power sharing approach using enhanced virtual impedance control scheme,” *IEEE Trans. Power Electron.*, vol. 28, no. 11, pp. 5272-5282, Nov. 2013.

[9] J. Kim, J. M. Guerrero, P. Rodriguez, R. Teodorescu, and K. Nam, “Mode adaptive droop control with virtual output impedances for an inverter-based flexible AC microgrid,” *IEEE Trans. Power Electron.*, vol. 26, no. 3, pp. 689-701, Mar. 2011.

[10] X. Wang, J. M. Guerrero, Z. Chen, and F. Blaabjerg. “Distributed energy resources in grid interactive AC microgrids,” The 2nd IEEE international symposium on power electronics for distributed generation systems. 2010. pp. 806-812.

[11] C. N. Rowe, T. J. Summers, R. E. Betz, D. J. Cornforth, and T. G. Moore, “Arctan power-frequency droop for improved microgrid stability,” *IEEE Trans. Power Electron.*, vol. 28, no. 8, pp. 3747-3759, Aug. 2013.

[12] Z. Chen, Y. Hu. “Control of power electronic converters for distributed generation units,” Proc. of the 31th annual conference of the IEEE industrial electronics society, IECON.2005, pp. 1317-1322.

[13] D. Feng, Z. Chen. “System Control of Power Electronics Interfaced Distribution Generation Units”, Proceedings of 5th International Power Electronics and Motion Control Conference, IPEMC 2006, Aug. 2006, Shanghai, China, pp.1-6

[14] Il-Yop. Chung, W. X. Liu, D. A. Cartes, and E. G. Collins, “Control methods of inverter-interfaced distributed generators in a microgrid system,” *IEEE Trans. Ind. Appl.*, vol. 46, no. 3, pp. 1078-1088, May/Jun. 2010.

[15] M. Hua, H. Hu, Y. Xing, and J. M. Guerrero, “Multilayer control for inverters in parallel operation without intercommunications,” *IEEE Trans. Power Electron.*, vol. 27, no. 8, pp. 3651-3663, Aug. 2012.

[16] C-T. Lee, C. C. Chu, and P-T. Cheng. “A new droop control method for the autonomous operation of distributed energy resource interface converters,” *IEEE Trans. Power Electron.*, vol. 28, no. 4, pp. 1980-1993, Apr. 2013.

[17] J. Rocabert, A. Luna, F. Blaabjerg, and P. Rodriguez, “Control of power converters in AC microgrids,” *IEEE Trans. Power Electron*., vol. 27, no. 11, pp. 4734-4749, Nov. 2012.

[18] A. H. Etemadi, E. J. Davision, and R. Iravani, “A decentralized robust control strategy for multi-Der microgrids- Part Ⅰ: fundamental concepts,” *IEEE Trans. Power Del.*, vol. 27, no. 4, pp. 1843-1853, Oct. 2012.

[19] A. L. Dimeas, and N. D. Hatziargyriou, “Operation of a multiagent system for microgrid control,” *IEEE Trans. Power Syst.*, vol. 20, no. 3, pp. 1447-1455, Aug. 2005.

[20] T. L. Vandoorn, C. M. Ionescu, and J. D. M, “Theoretical analysis and experimental validation of single-phase direct versus cascade voltage control in islanded microgrids,” *IEEE Trans. Ind. Electron.*, vol. 60, no. 2, pp. 789-798, Feb. 2013.

[21] A. Mehrizi-Sani, and R. Iravani, “Potential-function based control of a microgrid in islanded and grid-connected models,” *IEEE Trans. Power Syst.*, vol. 25, no. 4, pp. 1883-1891, Nov. 2010.

[22] A. Bidram, A. Davoudi, F. L. Lewis, and J. M. Guerrero, “Distributed cooperative secondary control of microgrids using feedback linearization,” *IEEE Trans. Power Syst.*, vol. 28, no. 3, pp. 3462-3470,

This article has been accepted for publication in a future issue of this journal, but has not been fully edited. Content may change prior to final publication. Citation information: DOI 10.1109/TPEL.2014.2345696, IEEE Transactions on Power Electronics





Aug. 2013.

[23] H. Xin, Z. Qu, J. Seuss, and A. Maknouninejad, “A self-organizing strategy for power flow control of photovoltaic generators in a distribution network,” *IEEE Trans. Power Syst.*, vol. 26, no. 3, pp. 1462-1473, Aug. 2011.

[24] X. Lu, J. M. Guerrero, K. Sun, and J. C. Vasquez, “An improved droop control method for DC microgrids based on low bandwidth communication with DC bus voltage restoration and enhanced current sharing accuracy,” *IEEE Trans. Power Electron.*, vol. 29, no. 4, pp. 1800-1812, Apr. 2014.

[25] Q. Shafiee, J. M. Guerrero, and J. C. Vasquez, “Distributed secondary control for islanded microgrid - a novel approach,” *IEEE Trans. Power Electron.*, vol. 29, no. 2, pp. 1018-1031, Feb. 2014.

[26] X. Wang, F. Blaabjerg, Z. Chen, and J. M. Guerrero. “A centralized control architecture for harmonic voltage suppression in islanded microgrids,” in IECON, pp. 3070–3075, 2011.

[27] D. A. Haughton, and G. T. Heydt, “A linear state estimation formulation for smart distribution systems,” *IEEE Trans. Power Syst.*, vol. 28, no. 2, pp. 1187-1195, May. 2013.

[28] Y. F. Huang, S. Werner, J. Huang, N. Kashyap, and V Gupta, “State estimation in electric power grids,” *IEEE Signal Processing Mag*, pp. 33-43, Sep. 2012.

[29] Y. Hu, A. Kuh, A. Kavcic, and T. Yang, “A Belief Propagation Based Power Distribution System State Estimator,” *IEEE computational intelligence magazine*, pp. 36-46, Aug. 2011.

[30] J. Liu, A. Benigni, D. Obradovic, S. Hirche, and A. Monti, “State estimation and branch current learning using independent local kalman filter with virtual disturbance model,” *IEEE Trans. Instrumentation and Measurement*, vol. 60, no. 9, pp. 3026-3034, Sep. 2011.

[31] Y. B. Wang, Y. J. Tian, X. F. Wang, Z. Chen, and Y. D. Tan, “Kalman-Filter-Based state estimation for system information exchange in a multi-bus islanded microgrid,” The 7th IET international conference on Power Electronics, Machines and Drives, Apr. 8-11. 2014.

[32] Y. B. Wang, X. F. Wang, Z. Chen, Y.J. Tian, and Y. D. Tan, “A communication-less distributed voltage control strategy for a multi-bus islanded AC microgrid,” The international power electronics conference-ECCE Asia- Japan, May. 18-21. 2014.

[33] L. C. Jin, R. Kumar, and N. Elia, “Model predictive control-based real-time power system protection schemes,” *IEEE Trans. Power Syst.*, vol. 25, no. 2, pp. 988-998, May. 2010.

[34] S. Bolognani, L. Peretti, and M. Zigliotto, “Design and implementation of model predictive control for electrical motor drives,” *IEEE Trans. Ind. Electron.*, vol. 56, no. 6, pp. 1925-1936, Jun. 2009.

[35] X. F. Wang, J. M. Guerrero, F. Blaabjerg, and Z. Chen, “Secondary voltage control for harmonic suppression in islanded microgrids,” in *Proc. IEEE PESGM*, 2011, pp. 1–8.

[36] N. Bottrell, M. Prodanovic, and T. C. Green, ‘‘Dynamic stability of a microgrid with an active load,’’ *IEEE Trans. Power Electron.*, vol. 28, no. 11, pp. 5107-5119, Nov. 2013.

[37] R. Majumder, B. Chaudhuri, A. Ghosh, R. Majumder, G. Ledwich, and F. Zare, “Improvement of stability and load sharing in an autonomous microgrid using supplementary droop control loop,” *IEEE Trans. Power Syst.*, vol. 25, no. 2, pp. 796-808, May. 2010.

[38] K. R. Muske, and T. A. Badgwell, “Disturbance modeling for offset-free linear model predictive control,” *Journal of Process Control*, vol. 12, pp. 617-632, Dec. 2002.

[39] U. Maedar, F. Borrelli, and M. Morari. “Linear offset-free model predictive control,” *Automatica*, vol. 45, pp. 2214-2222, 2009.

[40] C. A. Harrison, and S. J. Qin, “Discriminating between disturbance and process model mismatch in model predictive control,” *Journal of Process Control*, vol. 19, pp. 1610-1616, 2009.

[41] B. A. Francis, and W. M. Wonham, “The internal model principle of control theory,” *Automatica*, vol. 12, pp. 457-465, 1976.

[42] G. Welch, and G. Bishop, “An introduction to the kalman filter,” University of North Carolina at Chapel Hill, Chapel Hill, NC, 1995

[43] A. Bemprad, M. Morari, V. Dua, and E. N. Pistikopoulos, “The explicit linear quadratic regular for constrained systems,” *Automatica*, vol. 38, pp. 3-20, 2002.

[44] B. Huang, and R. Kadali, “Dynamic Modeling, Predictive Control and Performance Monitoring: A Data-driven Subspace Approach,” Springer Verlag, 2008.

**Yanbo Wang** was born in Gansu province, China, in 1986. He received the M.S. degrees in electrical engineering in the Electrical Engineering School, Southwest Jiaotong University, Chengdu, China, in 2011, where he is currently working toward the Ph.D degree. He was a Ph.D guest in the department of Energy Technology, Aalborg University, Denmark during Sep.2012 to Aug.2014.

His research interests include distributed power generation system, active distribution network, power system state estimation and stability analysis.

**Zhe Chen** (M’95–SM’98) received the B.Eng. and M.Sc. degrees from Northeast China Institute of Electric Power Engineering, Jilin City, China, and the Ph.D. degree from University of Durham, U.K.

Dr Chen is a full Professor with the Department of Energy Technology, Aalborg University, Denmark. He is the leader of Wind Power System Research program at the Department of Energy Technology, Aalborg University and the Danish Principle Investigator for Wind Energy of Sino-Danish Centre for Education and Research. His research areas are power systems, power electronics and electric machines, and his main current research interests are wind energy and modern power systems. He has led many research projects and has more than 360 publications in his technical field.

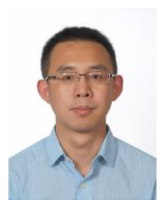

**Xiongfei Wang** (S’10-M’13) received the M.Sc. degree from Harbin Institute of Technology, Harbin, China, in 2008, in electrical engineering, and the Ph.D. degree in energy technology from Aalborg University, Aalborg, Denmark in 2013.

Since 2009, he has been with the Aalborg University, Aalborg, Denmark, where he is currently an Assistant Professor in the Department of Energy Technology. His research areas are in the harmonics analysis and mitigation in power electronics based power systems, system integration of renewable energy sources, and control of grid-connected converters.

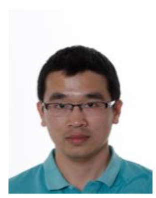

**Yanjun Tian** received the B.S. and M.S. degree in electrical engineering from the Yanshan University in China in 2009 and 2012. He is currently working toward the PhD degree in the department of Energy Technology in Aalborg University in Denmark.

His research interest is the active distribution network control, including the impedance interaction control, cascaded interface converter control and the parallel connected inverter control.

**Yongdong Tan** received the Ph.D. degree in electrical engineering in the Electrical Engineering School, Southwest Jiaotong University, Chengdu, China, in 2007.

He is currently a Professor in Electrical Engineering School, Southwest Jiaotong University. His research fields include autonomous decentralized system and control.

**Chao Yang** received the B.Eng. degree in electrical engineering from the Hubei University for nationalities, Hubei province, China, in 2009. He is currently working toward the Ph.D degrees at the College of Electrical Engineering, Chongqing University, Chongqing, China. His current research interests include operation and control of wind turbine generation system.